THESIS FOR THE DEGREE OF LICENTIATE OF ENGINEERING

Experimental study of a Volatiles Distributor for Improving the Cross-sectional Gas Distribution in Fluidized Beds

XIAOYUN LI

Department of Space, Earth and Environment

CHALMERS UNIVERSITY OF TECHNOLOGY

Gothenburg, Sweden 2022

Experimental study of a Volatiles Distributor for Improving the Cross-sectional Gas Distribution in Fluidized Beds

XIAOYUN LI

Department of Space, Earth and Environment

Division of Energy Technology

Chalmers University of Technology

SE-412 96 Gothenburg

Sweden

Telephone +46 (0)31-772 5248

Printed by Chalmers Reproservice

Gothenburg, Sweden 2022

Experimental study of a Volatiles Distributor for Improving the Cross-sectional Gas Distribution in Fluidized Beds

XIAOYUN LI
Division of Energy Technology
Department of Space, Earth and Environment
Chalmers University of Technology

Abstract

Chemical looping combustion (CLC) is a promising carbon capture technology due to its inherent CO_2 separation. Significant progress has been made in CLC of solid fuels in recent years. However, one key technical challenge for using solid fuels in CLC is to minimize the presence of unreacted gases coming from the fuel reactor together with CO_2, in particular for CLC of biomass, i.e. high-volatile fuel. Poor contact between volatiles and oxygen carriers is one reason for the lower gas conversion in the fuel reactor. Hence, the concept of a volatiles distributor (VD) is proposed for achieving a uniform cross-sectional distribution of volatiles, providing better gas-solid contacting and improving the gas conversion in the fuel reactor.

In this thesis, the VD was designed with different configurations and investigated in a cold-flow model under different fluidization velocities, volatiles flows and fluidization regimes. It was found that the VD gives a more uniform lateral distribution under higher fluidization velocity. Also, higher volatiles flow gives a more even distribution along the VD. It also shows that less open distribution area of the VD increases the pressure drop over the distribution holes, thus improving the lateral gas distribution. Moving holes from the vicinity of the volatiles injection towards the far end also improves the lateral distribution of volatiles even though it doesn't change the pressure drop over the distribution holes significantly.

The single bubble regime, i.e. large single bubbles formed at the bottom, and multiple bubble regime, i.e. multiple bubbles with different sizes formed at the bottom, were investigated with the VD. It was found that the VD gives a more uniform lateral distribution in single bubble regime compared to the multiple bubble regime. The installation of internal baffles at the bottom of the VD was found to reduce the bottom air flowing into the VD, thus improving the uniformity of the horizontal distribution of the volatiles and further reducing the risk of volatiles slip below the lower edge of the VD.

Keywords: Chemical looping combustion; Biomass; CO_2 removal; Fuel reactor; Volatiles distributor; Internal baffles; Gas-solid contacting; Fluidization regimes

ACKNOWLEDGEMENTS

The wonderful research journey about the volatiles distributor could have not been as successful without the help from many of you. First, I would like to thank my supervisor, Professor Anders Lyngfelt, who has always been there to answer my questions, discuss every detail of the problem, and wisely guide me to achieve a deep understanding. Second, I thank my examiner and main supervisor, Professor Tobias Mattisson, for constantly bringing in a new perspective and posing questions from a different angle, thereby enriching the discussions. I would also like to thank my co-supervisor, Senior Researcher Carl Linderholm, for his suggestions on my experimental work and efforts in critically reading and commenting on my papers.

I would like to thank Professor David Pallarès and Professor Bo Leckner for making time to answer my questions and providing me with valuable inputs on my theoretical and experimental research as well as on my papers. Furthermore, my deep gratitude goes to Ulf Stenman and Rustan Hvitt for helping me overcome the obstacles and achieve success in my experimental work.

I would like to acknowledge the Swedish Energy Agency (project number 46626-1) for the financial support of my work.

I am grateful to both Chemical Looping and Fluidization groups for the kind and continuous support. All the interesting presentations and discussions during the group meetings, but also the informal conversations, awaked even more interest in me for the research and made the work more joyful. I thank Daofeng, Amir, Carolina, Tove, Ivan, Ivana, Felicia, Nasrin, Victor, Fredrick, Mariane, and Guillermo for your suggestions, tips, and interesting discussions. I would also like to thank everyone from Energy Technology for creating this amazing, creative, encouraging, and energetic working environment. Every one of you is shining.

Last but most importantly, I would like to thank my big family and dear friends in China. Thank you all for always supporting me from the distance even though you have little idea about what I am doing in Chalmers. Especially I want to thank my elder brother, sister-in-law, cute nephew, and cousins for accompanying and caring for my parents and grandparents during these special years.

Xiaoyun Li, April 2022

List of Publications Included in the Thesis

This thesis is based on the following three appended papers:

Paper I

Xiaoyun Li, Anders Lyngfelt, Tobias Mattisson.

An experimental study of a volatiles distributor for solid fuels chemical-looping combustion process.

Fuel Processing Technology, 220 (2021) 106898.

Paper II

Xiaoyun Li, Anders Lyngfelt, David Pallarès, Carl Linderholm and Tobias Mattisson.

Investigation on the Performance of Volatile Distributors with Different Configurations under Different Fluidization Regimes

Energy & Fuels, (2022).

Paper III

Xiaoyun Li, Anders Lyngfelt, Carl Linderholm, Bo Leckner and Tobias Mattisson.

Performance of a volatiles distributor equipped with internal baffles under different fluidization regimes.

Manuscript Submitted for Publication (2022)

Xiaoyun Li is the principal author of Paper I-III and is responsible for the experimental work, data processing and evaluation, and authorship of the manuscripts for Paper I-III. Professor Anders Lyngfelt contributed with guidance in the experimental work, discussions and editing of Paper I-III. Professor Tobias Mattisson contributed with discussions and reviewing of the manuscripts for Paper I-III. Senior researcher Carl Linderholm contributed with discussions and reviewing of Paper II-III. Associate professor David Pallarès assisted in discussions and reviewing of Paper II. Professor Bo Leckner assisted in reviewing of Paper III.

Contents

CHAPTER 1

1. Introduction

1.1 Background

In recent years, with the higher frequency and intensity of weather extremes, climate change attracts more and more attention. The CO_2 concentration in the atmosphere increases steadily and reached an annual average 410 ppm in 2019[1]. In addition, there is still a huge amount of CO_2 emitted every year, corresponding around 40 $GtCO_2$/year in 2020[1]. The estimated budget for having a 66% chance of meeting the 1.5°C target is 420 Gt starting from January 2018[2]. This budget would be exhausted already around 2028 with the present CO_2 emission rate. Even though considerable efforts have been made to reducing greenhouse gas (GHG) emissions, it will still be difficult or perhaps even impossible to meet the Paris Agreement's temperature goal. Due to the near-linear relationship between cumulative anthropogenic CO_2 emissions and global warming, the global temperature will continue to increase until the net zero CO_2 emission target is reached. As the Intergovernmental Panel on Climate Change (IPCC) reports in the Sixth Assessment Report, global warming will exceed both 1.5 ^oC and 2 ^oC during the 21st century unless deep reductions in CO_2 and other greenhouse gas emissions occur in the coming decades[1]. Carbon removal technologies are necessary to meet the CO_2 budget in all scenarios considered by IPCC. Bioenergy carbon capture and storage (BECCS), considered to be the carbon removal technology with the highest potential, will play an important role if climate targets are to be achieved[3].

Chemical-looping combustion of biomass (Bio-CLC), as a promising BECCS technology, could play an important role for CO_2 capture since pure CO_2 can be

produced without the need of costly and energy-consuming gas separation. As shown in Figure 1, biomass absorbs CO_2 in air through photosynthesis and can be utilized by chemical looping combustion (CLC) to produce heat and power. CO_2 in air is captured by combining photosynthesis and CLC, and stored geologically to achieve the negative CO_2 emissions[4].

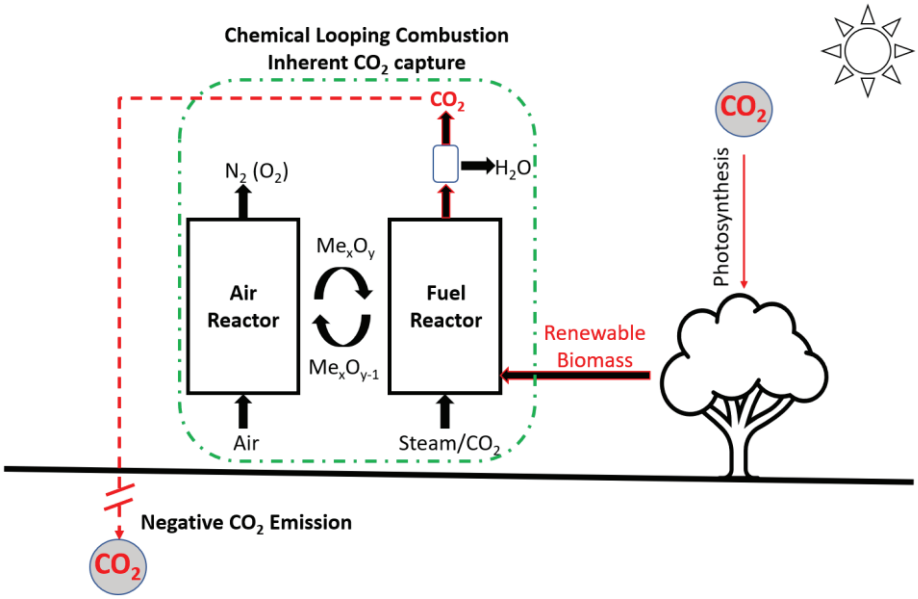

Figure 1. Negative CO_2 emission and power generation achieved by bio-CLC.

1.2 Chemical looping combustion of biomass

Bio-CLC as a BECCS technology attracts a lot of attention, since it separates conventional combustion into two steps, avoids the direct contact between fuel and air, and allows for inherent CO_2 separation without energy-intensive and costly CO_2 separation processes. As shown in the middle of Figure 1, the CLC process includes two interconnected fluidized-bed reactors, which are the air reactor and fuel reactor. Oxygen carriers (OC) are circulated between these two reactors in order to transfer oxygen from the air to the fuel and avoid the direct contact between them. The oxygen carrier is oxidized and takes oxygen from air in the air reactor and the oxidized oxygen carrier provides oxygen to convert the fuel in the fuel reactor in a N_2-free environment. Ideally, pure CO_2 is obtained after the condensation of steam in the flue gas of the fuel reactor and the energy penalty otherwise required for CO_2 separation from N_2 in the conventional combustion with BECCS is avoided. After the condensation of steam in the flue gas, the CO_2 can be compressed directly to be transported and then stored underground. However, a full conversion of the fuel in the fuel reactor is normally not

attained in the case of solid fuels. There are three likely deviations from the ideal case, incomplete gas conversion, char loss to the air reactor and elutriated char in the flue gas, as shown in Figure 2 [5]. And they are quantified by three performance indicators, i.e. oxygen demand, carbon capture efficiency and solid fuel conversion. Hence, understanding the conversion process of solid fuels in the fuel reactor and finding out a solution to improve the gas and char conversion inside the fuel reactor would be beneficial to CLC of solid fuels.

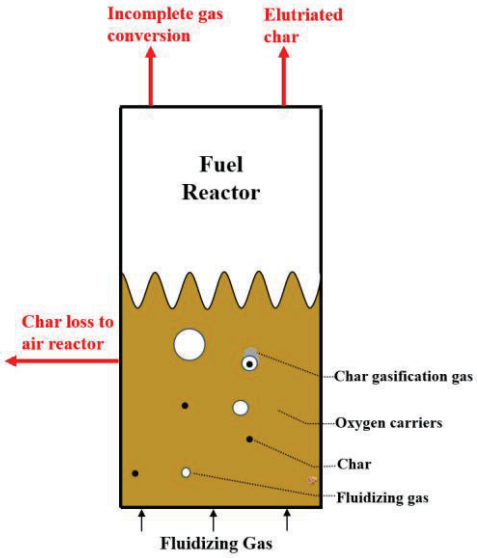

Figure 2. Inadequate performance of the fuel reactor[5].

The basic reactions in the fuel reactor (R1-R6) and air reactor (R7) for bio-CLC or CLC of solid fuels can be described as follows[6, 7].

$$\text{Solid fuel} \rightarrow \text{Volatile matter} + \text{Char} \quad \text{(R1)}$$

$$CH_4 + 4M_xO_y \rightarrow 4M_xO_{y-1} + CO_2 + 2H_2O \quad \text{(R2)}$$

$$C + H_2O \rightarrow H_2 + CO \quad \text{(R3)}$$

$$C + CO_2 \rightarrow 2CO \quad \text{(R4)}$$

$$CO + M_xO_y \rightarrow M_xO_{y-1} + CO_2 \quad \text{(R5)}$$

$$H_2 + M_xO_y \rightarrow M_xO_{y-1} + H_2O \quad \text{(R6)}$$

$$2M_xO_{y-1} + O_2 \rightarrow 2M_xO_y \quad \text{(R7)}$$

When solid fuels are injected into a fuel reactor at high temperature, the fuel is dried rapidly. After this, the devolatilization (R1) of the solid fuel takes place, typically within 1 s at 970 °C to generate char and volatiles for fuel particle sizes normally used in CLC ($< 250\mu m$)[6]. Subsequently, the volatiles, containing CO, H_2 and hydrocarbons, will

react directly with the oxygen carrier, e.g. R2, R5 and R6. The gasification (R3 and R4) of the char might take several minutes to generate H_2 and CO which can react with oxygen carriers directly (R5 and R6). Then the reduced oxygen carriers in the fuel reactor will be transferred to the air reactor and oxidized by the air (R7). Finally, the oxidized oxygen carriers can be looped back to the fuel reactor to react with the fuels.

Unburnt char may be transferred to the air reactor together with oxygen carriers, which will affect the carbon capture efficiency of the process. A carbon stripper has been proposed and optimized to separate the unburned char from the oxygen carriers in order to improve the carbon capture efficiency of the whole process. Kramp et al. investigated the performance of a carbon stripper by simulations, indicating an improvement of the carbon capture efficiency of CLC of solid fuels from below 50% to more than 90%[8]. Sun et al. investigated the performance and operations of different carbon strippers experimentally, which gives a base for the carbon stripper application[9, 10]. Different designs of carbon strippers have been demonstrated in different scales of CLC units[11-13]. Important for reaching high CO_2 capture is sufficient fuel reactor temperature and use of small fuel particle sizes. Pilot operation with biomass has demonstrated it is possible to reduce the loss of carbon to the air reactor to less than 1-2%[14].

Unconverted combustibles can be observed at the outlet of the fuel reactor, which are also critical for the performance of CLC especially for high-volatile fuels like biomass. There are two sources of these unconverted gases, i.e. char gasification products and volatiles. Char gasification products could be oxidized more or less completely because of the slow gasification process and good contact with the oxygen carriers[15]. A huge amount of volatiles would be formed after devolatilization since biomass has high content of volatiles. The substantial volatiles release in combination with the upwards flow direction of the fluidization gas may lead to a strong local plume of reducing gas near the biomass injection port. This will yield a limited contact between the volatiles and oxygen carriers in the fuel reactor bed and thereby a large amount of volatiles may leave the reactor unconverted.

Linderholm, et al,[6] investigated the CLC of solid fuels with different volatiles contents in a 10 kW unit, and found a much lower gas conversion rate of solid fuels with higher volatiles content, which indicates that the volatiles released from the solid fuel have insufficient contact with the oxygen carriers in the fuel reactor. A comparison of different fuel feeding positions, above-bed and in-bed, showed that in-bed fuel feeding method can increase the contact between the volatiles and the oxygen carriers which significantly improves gas conversion[6]. Similarly the gas conversion in a 100

kW unit using low-volatile fuel was high[12]. Ströhle et al.[16] investigated the performance of CLC of Calenturitas coal in a 1 MW_{th} unit, and found significant amounts of combustible gases in the fuel reactor exit, which resulted from the incomplete conversion of devolatilization and gasification products due to the limited gas/solid contact in the fluidized bed. Another MW-scale operation on bio-CLC also indicates that the volatiles conversion is to a significant extent limited by the mixing[17]. Petersen and Werther modelled a circulating fluidized-bed gasifier for sewage sludge, which has high volatiles content, and found that plumes with high pyrolysis gas concentrations was formed in the vicinity of the fuel feeding port and lateral mixing of the gas was not complete[18].

Going from small pilots to large-scale will greatly increase the cross-section area of fluidized-beds, and the volatiles can be expected to form a stronger local plume over the fuel entry, with the consequence of reduced contact between volatiles and oxygen carriers. There is thus a need to develop an effective and efficient solution that can improve the contact between the volatiles and the oxygen carriers in order to reach a higher gas conversion.

1.3 Methods for improving gas conversion in fuel reactor

There are several ways to decrease or remove remaining combustibles in the flue gas of the fuel reactor. Firstly, unconverted gases can be addressed by addition of pure oxygen at the outlet of fuel reactor, which is called oxygen polishing[19]. However, the presence of unconverted gases should be minimized to reduce the cost of oxygen production[5].

Secondly, more reactive oxygen carriers could also improve the fuel conversion in the fuel reactor. More than 70 different oxygen carriers have been tested in actual operation of CLC pilots, of which more than 3000 h are with solid fuels[15]. Oxygen carriers for solid fuels being studied range from low-cost to high-reactivity materials, i.e. ilmenite, iron ores, manganese ores or synthesized oxygen carriers[20-25]. Some ores and waste materials have reasonable cost and show reactive potential[26-28]. Some synthetic materials have shown higher potential to improve the fuel conversion in the fuel reactor[29-31]. Chemical-looping with oxygen uncoupling (CLOU) is a method proposed for improved or even full gas conversion in fuel reactor, since CLOU oxygen carriers can release gaseous oxygen, which can react with solid, liquid and gaseous fuels[32]. Mattisson et al.[32] and Leion et al.[33] showed that the conversion rate of

solid fuels can be improved significantly by CLOU compared to conventional CLC. Various kinds of CuO-based, Mn-based and perovskite-type oxygen carriers, synthesized with different supporting materials and different manufacturing techniques, were studied, and showed high O_2-uncoupling capacity, sufficient reactivity and mechanical strength[34-40]. Full fuel conversion in the fuel reactor has been achieved by using copper or copper manganese mixed oxides[41, 42]. However, different drawbacks of the above-mentioned CLOU oxygen carriers, such as the susceptibility to sintering and agglomeration, limited mechanical strength, slow oxidation kinetics and the deactivation due to impurities in the fuel[43-47], and production costs may potentially make CLOU materials less attractive for large-scale implementation. A trade-off should be made between the reactivity and the lifetime or cost of the oxygen carriers due to the loss of oxygen carrier particles with the ash leaving the system.

Thirdly, different designs and modifications of the fuel reactor have been proposed aiming for higher fuel conversion. A two-stage fuel reactor was proposed and proved to have better combustion performance compared to previous CLC facilities[48]. Internals, i.e. vertical or horizontal tubes, fitted in fluidized-beds reduce bubble size, increase the emulsion voidage, and thereby increase the overall residence time of reactant gas in the bed[49]. Massimilla and Johnstone found that a fluidized-bed with baffle grids had much higher gas conversion than the non-baffled fluidized-bed[50]. Guío-Pérez et al.[51] investigated the influence of ring-type internals equipped inside the fuel reactor, which showed positive effect on the solids residence time. Pérez-Vega et al.[52] modified the fuel reactor of a 50 kW_{th} unit by the ring-type internals in the upper part of the reactor with the objective of improving the solids distribution and enhancing the gas-solid contact. An improved gas conversion is achieved. However, the effects of such internals may be less in large-scale units with bigger cross-sections.

1.4 Fluidization regime at bottom of fuel reactor

Typically, the CLC process is realized by a system of two interconnected fluidized beds, since fluidized beds provide well-controlled operations, good mixing of solids and high solid-gas contacting efficiency. The air reactor is used for oxidizing the reduced oxygen carriers and also transports the oxidized oxygen carriers to the following cyclone leading to the fuel reactor. Hence, circulating fluidized-bed reactors are used for air reactors. They are usually designed as a single riser or a wide bottom bed together with a narrow riser as presented in Figure 3. The wide bottom bed usually exhibits a turbulent

fluidization regime and the riser is in the pneumatic transportation regime[53]. However, the reaction pattern in the fuel reactor is much more complex compared to the air reactor. Complete fuel conversion in the fuel reactor is desired in the CLC process. A huge amount of volatiles would be formed in the fuel reactor, in particular for bio-CLC, and therefore good contact between volatiles and oxygen carriers is needed. The gas-solid contacting is strongly related to the fluidization regime established in the bottom dense bed, where devolatilization, char gasification and oxidation of the gasification products or volatiles mainly take place. The hydrodynamics of the bottom bed in the fuel reactor are therefore of great interest.

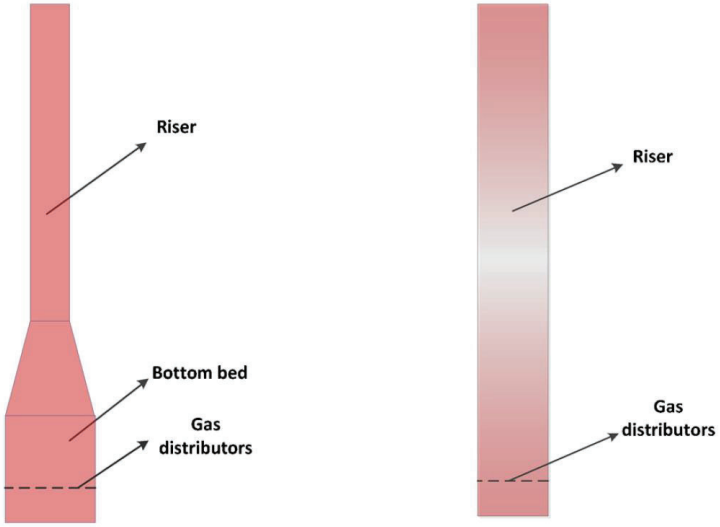

Figure 3. Scheme of an air reactor in CLC system. Left: a wide bottom bed with a narrow riser; Right: a single riser[53].

Bubbling fluidized beds[11, 54-60] and circulating fluidized beds[61-67] are widely used for the design of the fuel reactor from small lab-scale units to MW-scale units. Bubbling fluidized bed requires less superficial fluidization velocity. But the combustibles produced may bypass the dense bed through the bubbles without contacting the oxygen carriers. Further, there is less gas-solid reactions in the freeboard above the dense bed due to the lower solids holdup in this region. This is a shortcoming of using bubbling bed for the fuel reactor, which could be fixed by increasing the solids inventory in the fuel reactor to extend the gas-solid contacting time. However, higher ratio between the bed height to the bed diameter could cause slugging problems relevant for small units. A circulating fluidized bed riser can provide a more homogeneous solids distribution over the height of the riser, which ensures good gas-solid contacting. Further, the pressure drop over the gas distributor between the wind box and the dense bed is also closely related to the fan energy consumption even though the same superficial gas velocity is used. However, most publications do not report any

information about the pressure drop over the air distributor, which may give different fluidization regimes in the dense bed, i.e. single bubble regime and multiple bubble regime[68, 69]. Moreover, commercial boilers are normally operated with a moderate pressure drop over the air distributor due to economic interests, yielding the single bubble or exploding bubble regime at low and higher fluidization velocity, respectively[69].

The common practice in fluidized-bed boilers is to feed the fuel above the dense bottom zone. In CLC, however, it is desired that gases from the fuel are released as far down in the bed as possible in order to achieve good contact between volatiles and oxygen carriers. Hence, solid fuel in-bed feeding or at the loop-seal connecting to the fuel reactor are favorable. The volatiles released rapidly from the solid fuel in the dense bed may also have an influence on the gas-solid contacting regime in the fuel reactor. Lyngfelt and Leckner[5] described the gas velocity changing with the fuel reactor height as presented in Figure 4. In a real-world fuel reactor of commercial size, the bottom fluidization gas flow would be expected to be low. The bottom gas, either steam or a combination of steam and recycled CO_2, comes with a significant cost, and its major purpose is to keep the bed fluidized. Thus, the optimal bottom gas flow is likely the minimum flow needed to safely achieve adequate fluidizing conditions. Apart from the bottom fluidization gas flow, there are two major gas flows in the fuel reactor originating from the char and the volatiles. The char will mainly be part of the dense phase. Thus, the syngas produced by gasification will also appear in the dense phase. This will make the dense phase “self-fluidizing”, which is likely to change the bottom bed to turbulent regime and be helpful for improving the gas-solid contacting.

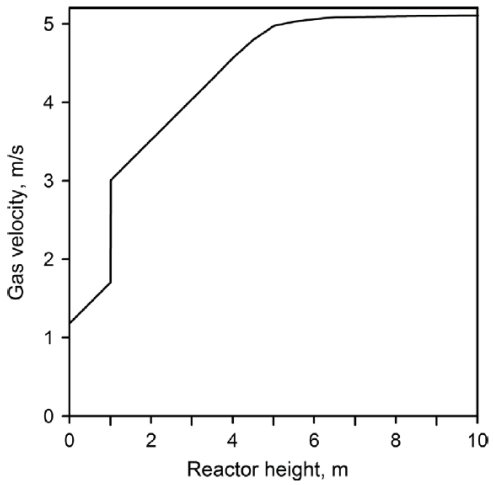

Figure 4. Gas velocity in fuel reactor versus height.

1.5 Aim and scope of this thesis

In the fuel reactor, a local plume of volatiles released rapidly from the solid fuel in the fuel reactor may cause poor gas-solid contacting and thus lower the gas conversion in the fuel reactor. Such a plume would be more pronounced going from small-scale to commercial size units with high-volatile fuels, i.e. biomass. The aim of this work is to introduce and investigate a novel concept called volatiles distributor aiming for a more even distribution of volatiles at the bottom of the fuel reactor and better contact between volatiles and oxygen carrier, and thus improve combustion efficiency. In this way, the ultimate purpose is to lay the foundation for future large-scale implementation of the volatiles distributor concept, in order to improve lateral mixing of the gas and thereby gas conversion in fluidized beds, of central importance for technologies like CLC, but also applicable for other fluidized bed technologies. Although the concept has been proposed previously, this is the first comprehensive investigation of the functionality of such a system.

This thesis summarizes the investigation of the VD in a cold-flow fluidized-bed model in Paper I - III. Different designs and modifications of the VD are investigated under different operational conditions and fluidization regimes in the cold-flow fluidized-bed model. The performance of the VD with respect to the uniformity of the lateral distribution of volatiles is analyzed and evaluated.

CHAPTER 2

2. Theory and Experimental Method

2.1 Concept of volatiles distributor

If a box with an opening downwards is immersed in a fluidized bed, it is known that the inside of the box will be free of bed materials and the bed surface level will be at the bottom edge of the box. However, if holes are made in the sides of the box, the bed level inside the box will increase to the level of the holes and the fluidization gas can pass through the holes as shown in Figure 5. If a gas is injected into this box above the side holes level, it will pass through the holes creating a pressure drop over the holes. The increased pressure will lower the bed level inside the box.

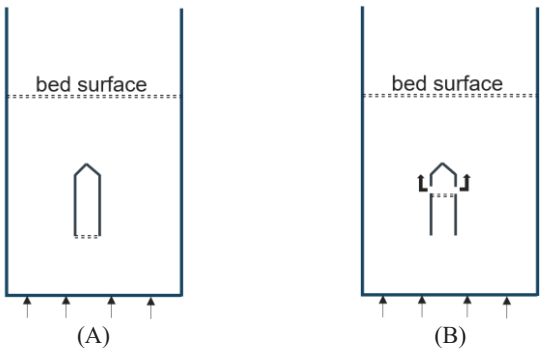

Figure 5. Box immersed in a fluidized-bed. (A) without holes in the sides, (B) with holes in the sides.

Such a box can be extended to an arm and if a system of such arms is built and extended across the cross-section of a fluidized-bed, gases can be distributed via the holes in the sides across the whole cross-section. Furthermore, this system can also be connected to the fuel feeding, in order to distribute the volatiles over the cross-section[5]. An example of VD design is shown in Figure 6, having eighteen long and narrow boxes,

i.e. arms, with openings downwards that are immersed at the bottom of a fluidized bed. The arms collect the volatiles released from the fuel fed between the downcomer and the fuel reactor. The remaining char will be mixed with the bed material. If these arms would only be open downwards, the inside of the arms will be free of bed material and the volatiles would flow into the bed below the lower edge of the arms. However, if holes are made in both sides of the arms along the length, volatiles can flow into the arms and pass through the holes. Bed particles would be present in the arms and form a dense bed inside the arms below the level of the holes. If the fuel is injected between the downcomer and the fuel reactor and devolatilized immediately, the volatiles shown in green in Figure 6 will thus flow from the freeboard into the upper part of the arms and pass through the holes together with some fluidization gas from the bottom. The box and associated arm-construction described above could be a good way of avoiding plume formation and enabling a more homogeneous distribution of volatiles across the cross section of the fuel reactor. The principle can also be relevant for other purposes, like thermal gasification using dual fluidized-beds.

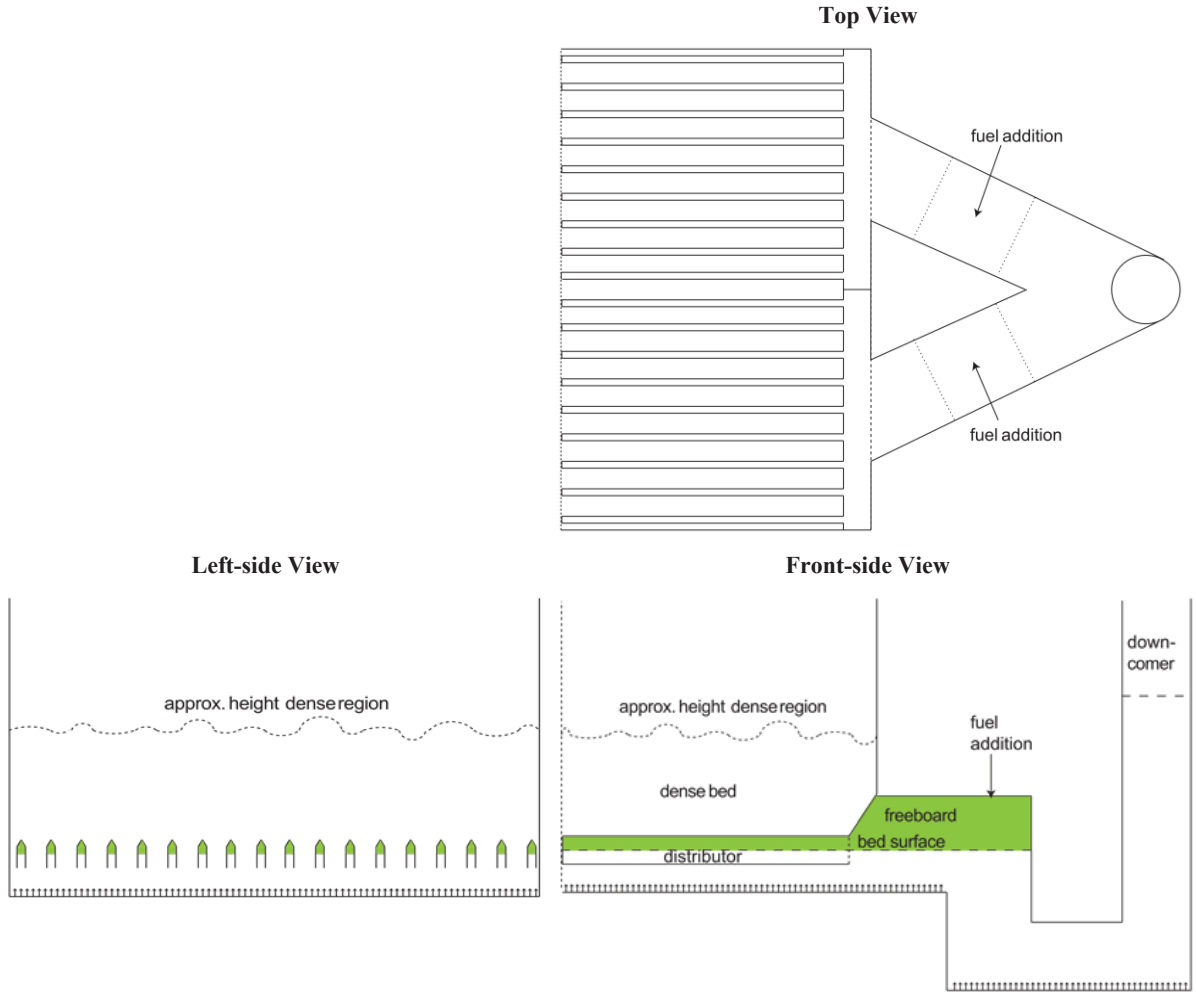

Figure 6. Illustration of the volatiles distributor arrangement in a fluidized bed.[5]

2.2 Experimental system

The cold-flow fluidized-bed model includes a wind box, a riser and a cyclone. The riser has a length × width × height of 700 mm × 120 mm × 8500 mm. The front side of the riser is made from Perspex glass which allows visual observation of fluidization inside the VD. The VD is installed at the bottom of the riser at a height of 114 mm, i.e. from the bottom of the VD to the bottom of the riser. The fluidization air is provided by fans. In this work, the volatiles are simulated using a mix of air and CO_2 as a tracer gas. There is an injection hole for simulated volatiles at the front plate, which allows the simulated volatiles to flow into the VD, cf. Figure 7.

Along the height of the riser, there are twenty-four taps for pressure measurements, which are installed in the middle of the backside of the riser. The pressure measurement in the wind box is located at the right side, shown as a pink point in the right top corner of the wind box in Figure 7 (a). There are two more pressure taps to measure the pressure drop between the inside and outside of the VD, one of which is in the middle of backside of the riser at the same height as the distribution holes, i.e. 374 mm. The other one is for the pressure measurement inside the VD, which is to the right top corner of the front plate, i.e. the pink crossed circle shown in the gas sampling tube position of Figure 7 (b).

There are thirteen gas sampling tubes in the experimental system, which are the higher-level ones (HSV1-HSV6), the lower-level ones (LSV1-LSV6) and the one for sampling the gas inside the VD. The latter is located in the top right corner of the front plate, shown as a pink crossed circle shown in Figure 7 (b). The gas sampled from the tubes passes filters, and flows through the pump and the gas analyzer in the following sequence: LSV6, LSV5, LSV4, LSV3, LSV2, LSV1, HSV6, HSV5, HSV4, HSV3, HSV2, HSV1 and finally the top right corner of the VD. The flowrate is 1 L_n/min. For each measurement position, the gas flows into the gas analyzer for 210 s in total, the first 90 s is for stabilization and the remaining 120 s is for recording data to calculate the average concentration.

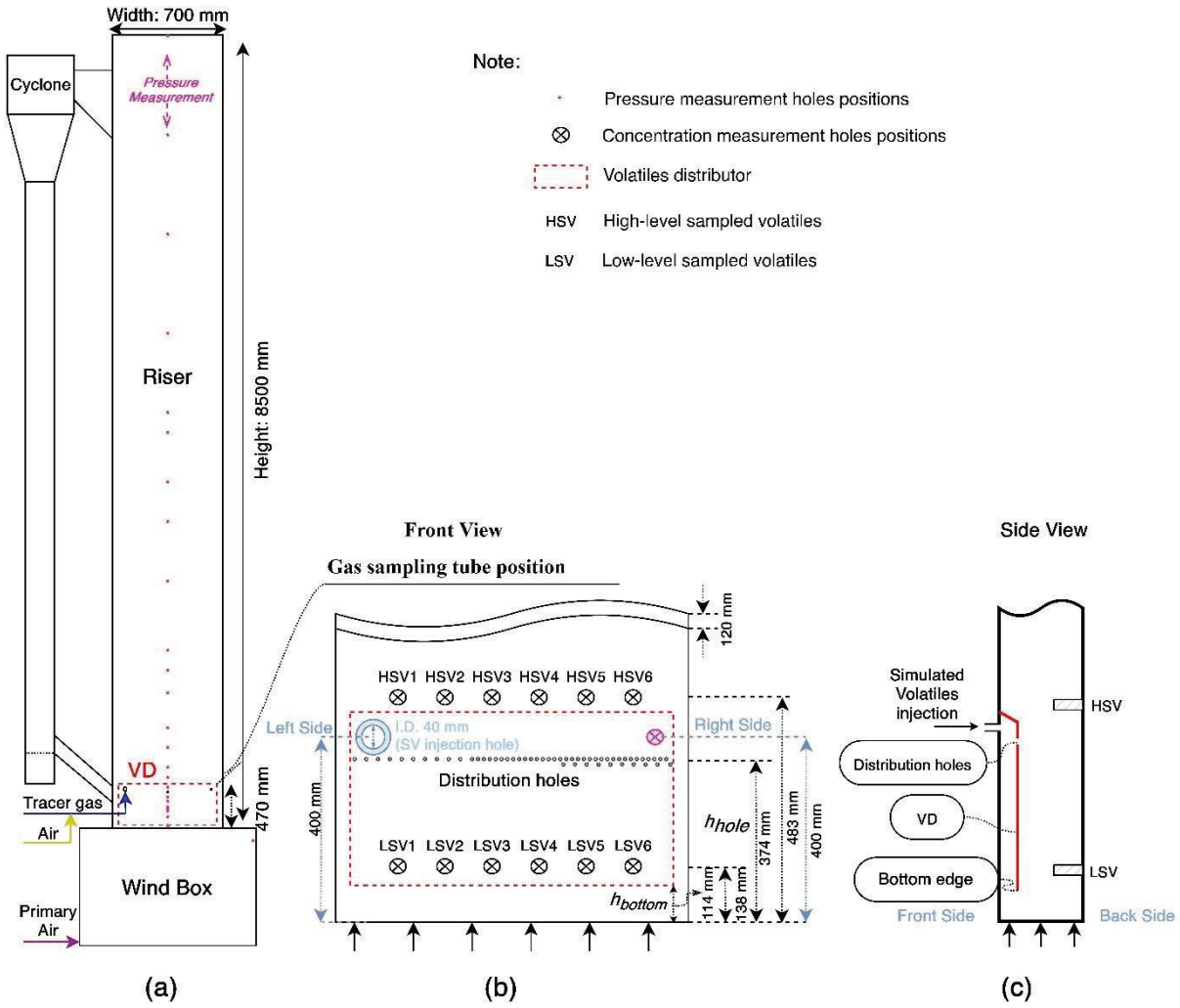

Figure 7. (a) Cold-flow circulating fluidized-bed model equipped with the VD and pressure and CO_2 concentration measurement systems; (b) Front view of the riser bottom, the distribution holes are seen in detail in Figure 8; (c) Side view, the side view with more details is shown in Figure 10.

2.3 Designs of a volatiles distributor

The performance of the VD was investigated in this cold-flow fluidized-bed model. Figure 8 presents the sketch of the VD, which is attached on the bottom front plate of the fluidized bed. The design of the distribution holes, i.e. the arrangement of the holes and the open area of the holes, is vital to the performance of the VD on the horizontal distribution of the volatiles. Hence, different configurations of the distribution holes (Mode A and Mode B) and different open areas of the distribution holes (Mode 1 and Mode 2) were investigated in this work. Mode 1A and Mode 1B have the same open area and number of holes, i.e. 58 holes, but different distribution of the holes. Mode 1A has the evenly distributed open area along the length of the VD. However, Mode 1B has less open area at the left side, i.e. the volatiles injection side but more at the right

side, i.e. far away from the volatiles injection side. Mode 2A and Mode 2B have similar arrangements as Mode 1A and Mode 1B except that Mode 2A and Mode 2B have the double open area as well as double number of holes, i.e. 116 holes. The diameter of the distribution holes is 5 mm.

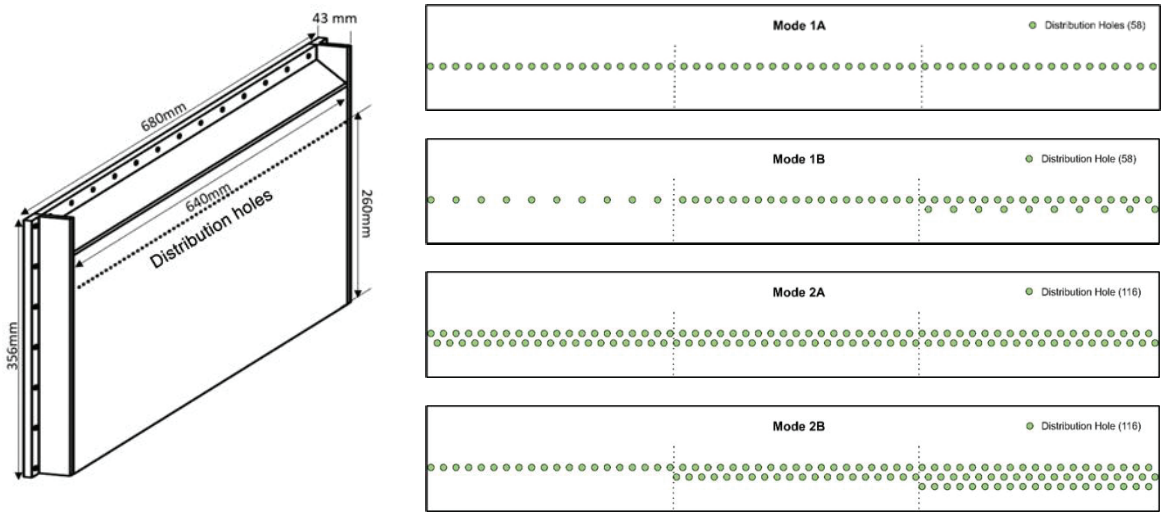

Figure 8. Sketch of the VD and different configurations of the distribution holes.

The internal baffles were designed based on the hourglass concept, and the idea with these was to improve the performance of the VD by reducing the solids movement inside the VD, i.e. to promote a more even volatiles distribution and less risk of volatiles slip below the lower edge of the VD close to the volatiles inlet. As shown in Figure 9, the cross section of the internal baffle is narrowing down from the bottom to the top. If the bottom of the VD is equipped with a series of internal baffles, the bed materials inside the VD will fall down through the space between each two adjacent internal baffles more slowly. Likewise, upwards movement of bed material will also be slowed down. The arrangement of the internal baffles inside the VD is shown in Figure 9. The length of each internal baffle is 40 mm. The length of VD bottom is 624 mm. Hence, the ten internal baffles occupy 64.1% of the cross section at the bottom of the VD.

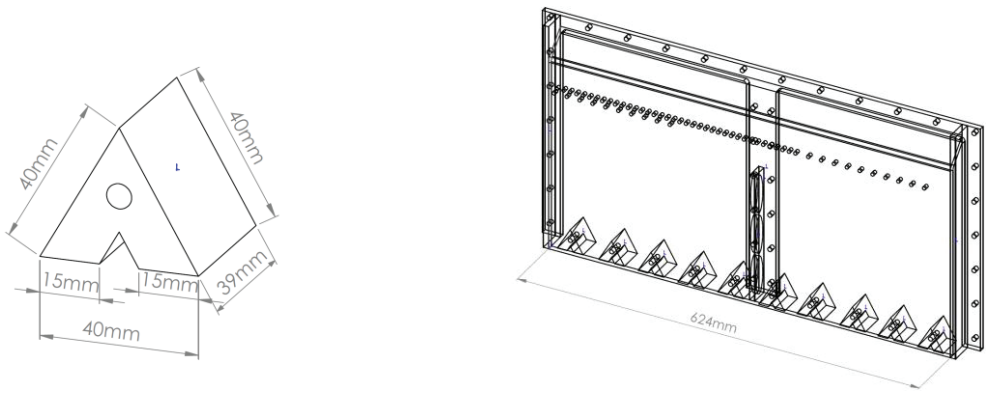

Figure 9. The design of internal baffles and arrangement at the bottom of the VD.

2.4 Bed material

Glass beads are used as bed material for this study, having a density of 2600 kg/m^3 and a particle size range from 250 μm to 425 μm, which is similar to the bed materials used in boilers[70]. These solids belong to Group B in the Geldart classification. The average particle diameter is 316 μm, corresponding to a single particle terminal velocity of 2.21 m/s. The minimum fluidization velocity is 0.067 m/s[70]. In each experiment, 100 kg of solids were filled into the riser.

2.5 Operational conditions

Fluidization velocity is one of the most important parameters in the field of fluidization. The flow of simulated volatiles can represent the fuel injection rate to some extent. Hence, the performance of the VD was investigated under different fluidization velocities and simulated volatiles flows as presented in Table 1. The different flows of simulated volatiles, i.e. volatiles percentage, are achieved by changing both the CO_2 flow and air flow for simulating the volatiles. The pressure drop over the air distributor plays an important role for the fluidization regime in the riser. Therefore, an investigation of the performance of the VD with different air distributors, i.e. an air distributor with 198 holes (AD198) and an air distributor with 1660 holes (AD1660), was performed in order to identify how the VD performs under different fluidization regimes. A more detailed discussion about the different types of regimes can be found in the references[69, 71]. The performances of the VD with different configurations of the holes for distribution, were also compared. The modification of the VD with internal baffles aiming for a more even horizontal distribution and less risk of volatiles' bottom slip, was applied and evaluated as well in this work. The overview of the experimental conditions is presented in Table 1.

Table 1. Overview of the operational conditions.

Air distributor	Volatiles distributor	Internal baffle	Fluidization velocity u_0 [m/s]	Volatiles percentage $\frac{V_{sv}}{V_{sv}+V_{pa}}$	Investigated parameters
AD1660	Without Mode 1A	Without	0.9, 1.8, 2.8, 3.7	10%, 20%, 30%	**Fluidization velocity** **Volatiles percentage** (Paper I[72])
AD1660	Mode 1B Mode 2A Mode 2B	Without	0.9 3.7	10% 30% 10%	**Fluidization regime** **Configuration of distribution holes** (Paper II[71])
AD198	Without Mode 1B Mode 2B	Without	0.9 0.6	30% 30%, 40%	
AD198 AD1660	Mode 1B Without Mode 1B	With Without With	0.6 0.6 3.7	30%, 40% 30% 40% 10%	**Internal baffles** (Paper III[73])

CHAPTER 3

3. Data Processing and Analysis

The results through Paper I to III are mainly based on the recorded data from the pressure and tracer gas concentration measurements.

Solids concentration, pressure fluctuations, and height of dense bed can be obtained from the pressure measurements along the height of the riser and the inside of the volatiles distributor. The horizontal distribution of the simulated volatiles can be obtained from the tracer gas, i.e. CO_2 concentration measurements.

In this section, evaluation parameters derived from the pressure and concentration measurements results are presented.

3.1 Solids concentration

The solids concentration at a certain height can be estimated by pressure measurements along the height of the riser. The pressures are the averages at different measurement positions during a given period. The average solids concentration, $c_{s,h_{1\to2}}[\mathrm{kg/m^3}]$ between two pressure measurement positions, h_1 and h_2, can be estimated as follows[74]. First, the voidage is calculated using the general expression for the pressure drop:

$$\left|p_{h_1} - p_{h_2}\right| = (\rho_s(1 - \varepsilon_{g,h_{1\to2}}) + \rho_g \varepsilon_{g,h_{1\to2}})g|h_1 - h_2| \quad (1)$$

Then the average solids concentration in this height interval is given by:

$$c_{s,h_{1\to2}} = \rho_s(1 - \varepsilon_{g,h_{1\to2}}) \quad (2)$$

3.2 Power spectral analysis

Power spectral analysis is often used to determine the dominant frequencies and the frequency distributions of pressure fluctuations in fluidized bed, which can be applied to identify the fluidization regime transitions and validate the hydrodynamic scaling relationships between the pilot-scale and the full-scale units[75, 76]. In this thesis, power spectral analysis of the pressure fluctuations signals by Fast Fourier transform (FFT), being a more objective method compared to the time domain analysis, is used to characterize the fluidization regime.

Assume that the time series of the variance in the pressure signals is divided into L segments with a length of N_s for each segment, and those segments are represented as:

$$x_i(n) = x(n + (i-1)N_s), \quad n = 1,2,\dots,N_s,\ i = 1,2,\dots,L. \quad (3)$$

The time series pressure signal $x(n)$ estimated as the Fourier transform of the autocorrelation sequence is expressed by:

$$F(f) = \sum_{n=1}^{N_s} x(n)e^{-j2\pi nf} \quad (4)$$

The power spectrum density (PSD) can be performed by using FFT, which is calculated from:

$$P_{xx}^{i}(f) = \frac{1}{N_s f_s}\left[\sum_{n=1}^{N_s} x(n)e^{-j2\pi nf}\right]^2 \quad (5)$$

Here the normalization factor $1/(N_s f_s)$ is used. f_s is the sampling frequency.

The average power spectrum is:

$$P_{xx}(f) = \frac{1}{L}\sum_{i=1}^{L} P_{xx}^{i}(f) \quad (6)$$

The number of discrete frequencies tested is proportional to the numbers of samples in each segment. The frequency resolution or intervals is $\Delta f = \frac{f_s}{N_s}$, i.e. 0.0244 Hz in this work. The highest frequency analyzed (named Nyquist frequency) is $f_s/2$, i.e. 25 Hz.

The pressure sampling frequency is 50 Hz in this work, which is sufficient to determine the frequency distribution since the major frequency range of pressure fluctuations is normally below 10 Hz[76]. All frequency spectra shown below are based on the average of 32 sub-spectra, each of which has 2048 samples, in order to ensure sufficient

accuracy. The pressure signals are from the measurements at the position 0.03 m above the air distributor and in the wind box.

3.3 Standard deviation of pressures

The standard deviation of pressures is one method to estimate the fluctuation amplitude, which is calculated as:

$$\sigma = \sqrt{\frac{\sum_{n=1}^{N}(x(n)-\bar{P})^2}{N}} \tag{7}$$

where N is the total number of data points, $\bar{P}$ is the average value and n = 1, 2, 3, …, N.

3.4 CO_2 ratio

In an ideal case, when the injected volatiles are perfectly mixed across the whole cross-section, the CO_2 concentration at different positions of the cross-section will be the same, which is called the ideal average CO_2 concentration in this thesis. The ideal average CO_2 concentration is calculated based on the CO_2 flow (MF_{CO_2} [m_n^3/h]), air flow used for simulating volatiles (MF_{SA} [m_n^3/h]) and primary air flow (MF_{PA} [m_n^3/h]) for the main fluidization.

$$c_{cal} = \frac{MF_{CO_2}}{MF_{CO_2}+MF_{SA}+MF_{PA}} \tag{8}$$

In order to compare the horizontal distribution of simulated volatiles in different cases statistically, a parameter named CO_2 ratio (R) was defined as the ratio between the measured CO_2 concentration (c_m [ppm], with CO_2 in ambient air subtracted) at each measurement position and the ideal average CO_2 concentration in the cross-section of the riser (c_{cal} [ppm]).

$$R = \frac{c_m}{c_{cal}} \tag{9}$$

A further analysis based on the CO_2 ratios at different positions of the higher level is conducted in order to evaluate the overall performance of the different volatiles distributors under different operational conditions with different air distributors. Here are the parameters used for the evaluations.

The average CO_2 ratio over the six horizontal measurement positions:

$$\bar{c}(c_1, c_2, \ldots c_n) = \frac{\sum_{i=1}^{n} c_i}{n} \quad (10)$$

The standard deviation of the CO_2 ratios:

$$SD = \sqrt{\frac{\sum_{i=1}^{n} (c_i - \bar{c})^2}{n}} \quad (11)$$

The relative standard deviation of the CO_2 ratios:

$$RSD = \frac{SD}{\bar{c}} \times 100\% \quad (12)$$

The ratio between the highest CO_2 ratio (c_H) to the lowest one (c_L) at the six positions of the higher level is also calculated, which is expressed as c_H/c_L.

3.5 Dense bed height estimation inside the VD

The bed material inside the VD is fluidized by the continuous bottom inflow from the main riser into the VD. The height of the dense bed inside the VD, h_b (see a sketch of the side view in Figure 10) is estimated from pressure measurements. Geometry gives:

$$h_b = h_{hole} - \Delta h - h_{bottom} \quad (13)$$

where h_{bottom} is the distance from the air distributor plate to the lower edge of the VD, h_{hole} is the distance from the distributor plate to the level of distribution holes of the VD, and Δh is the distance between the top of the dense bed surface inside the VD and the level of distribution holes. Δh can be estimated from the pressure difference between the inside VD and the main bed at the hole height, and the measured pressure gradient dp/dh on the outside of the VD is assumed to be similar to that inside the VD.

$$\Delta h = \frac{p_{in} - p_{out}}{|dp/dh|} \tag{14}$$

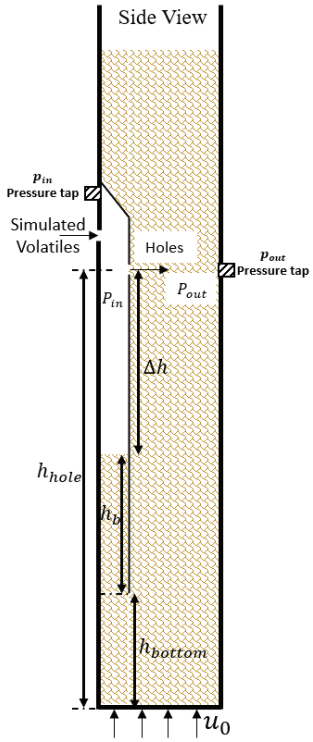

Figure 10. Sketch of the side view of the bottom part of the riser.

3.6 Dilution of volatiles inside the VD

The injected simulated volatiles would be diluted by the bottom air from the main fluidization. This dilution affects the horizontal distribution of the simulated volatiles. Therefore, the flow of fluidization air from the bottom entering the VD is estimated and the degree of the dilution to the injected simulated volatiles is also evaluated based on the dilution factors.

The calculation method is based on the calculation of the gas velocity through the orifice[77]. Once the pressure drop over the distribution holes, $p_{in} - p_{out}$, and the orifice discharge coefficient, C_d, are known, the gas velocity through the distribution holes of the VD can be estimated.

$$v_{orifice} = C_d \sqrt{\frac{2(p_{in} - p_{out})}{\rho_{gas}}} \tag{15}$$

Here, the gas density, ρ_{gas}, is 1.19 kg/m^3, and the value of C_d depends on the grid plate thickness, t, and the hole pitch, L_h. According to the relationship between $C_d(L_h/d_h)^{0.1}$ and thickness-to-diameter ratio in the grid hole discharge coefficient design

chart as shown in Figure 11[78], where d_h is the diameter of the holes, the value of C_d can be set to 0.92 in Paper III (it is simply assumed as 0.6 in Paper I and II), since L_h, d_h and t are 10 mm, 5 mm and 8 mm respectively.

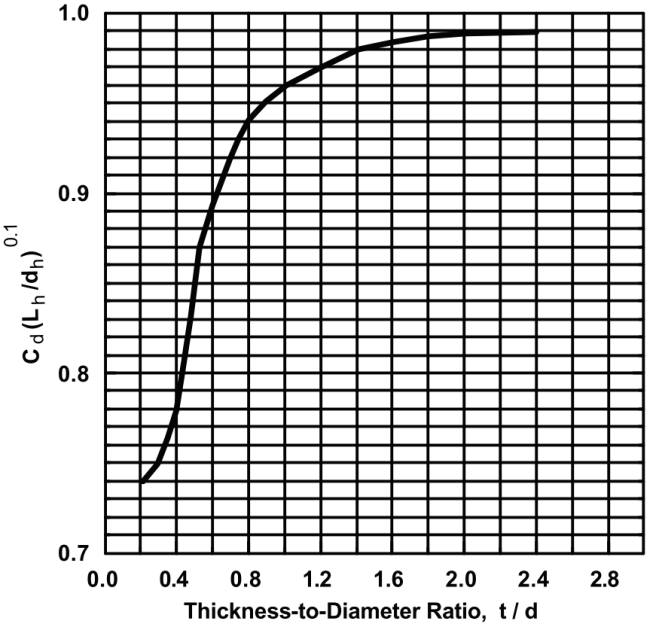

Figure 11. Grid hole discharge coefficient design chart[78].

Then, the total gas flow through the distribution holes is obtained knowing the open area $A_{orifice}$.

$$V_{orifice} = v_{orifice} \times A_{orifice} \tag{16}$$

The total gas flow through the distribution holes of the VD ($V_{orifice}$) includes the bottom air flow (V_{ba}) and the flow of injected simulated volatiles (V_{sv}). Hence, the bottom air flow is estimated as:

$$V_{ba} = V_{orifice} - V_{sv} \tag{17}$$

There are two ways to calculate the dilution factors. The first method is based on the flows of bottom air and injected simulated volatiles. The second method uses the CO_2 concentration in the injected simulated volatiles and the measured CO_2 concentration inside the VD. Hence, the dilution factors could be calculated as:

$$D_1 = \frac{V_{ba}}{V_{sv}} \tag{18}$$

$$D_2 = \frac{c_{vd}}{c_{sv}} = \frac{c_{vd}}{V_{CO_2}/V_{sv}} \tag{19}$$

Here, c_{vd} is the measured CO_2 concentration inside the VD at the top right corner.

CHAPTER 4

4 Results and Discussion

In this section, the results from the included papers are summarized, which highlight the main findings about the performance of the volatiles distributor with different configurations under different fluidization regimes.

4.1 Vertical profile of the solids concentration

The vertical profile of solids concentration in the riser gives a basic overview of the different fluid-dynamical zones. Figure 12 presents the vertical solids concentration profiles with and without the VD, obtained from the pressure measurements along the height of the riser. At the bottom of the riser, a dense bed region with constant solids concentration along the height is formed, and higher fluidization velocity gives lower solids concentration. Above the dense bed region, a splash zone is formed with an exponential decay in solids concentration, caused by the strong back-mixing by means of ballistic movement of clustered particles. A transport zone with lower exponential decay above the splash zone occupies most of the riser height and has a dispersed solids flow. Higher fluidization velocity transfers more bed materials from the bottom to the transport zone. Hence, higher fluidization velocity gives a lower bottom bed and increases solids concentration in the upper part of the riser compared to lower fluidization velocity.

It was found that the variation in solids concentration from the bottom to the top of the riser in the presence of VD is generally similar to what is seen in absence of VD at low fluidization velocity as shown in Figure 12. But there is one big difference in solids

concentration profile at higher fluidization velocity between with and without the VD. With VD, the solids concentration at the bottom when using a fluidization velocity of 3.7 m/s, decreases up to 300 mm height, and then increases up to 470 mm, which is exactly the top end of the VD. The presence of the VD gives a higher velocity locally, which approximately halves the concentration in this height range. This rise in velocity is significant, because the VD occupies one third of the cross-section. In a real-world application this fraction could be smaller.

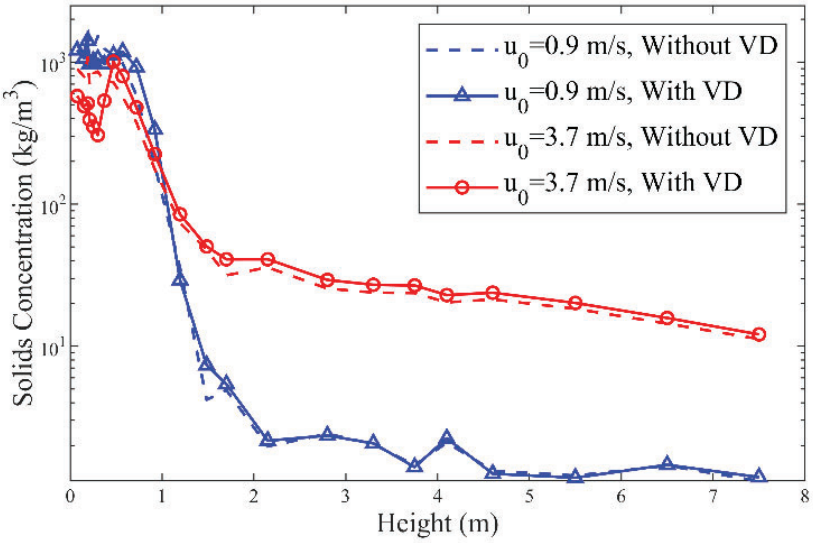

Figure 12. Solids concentration profile under different fluidization velocities in absence and presence of the VD with configuration Mode 1A.

It was also found that the solids concentration profile along the riser height remains similar when the configuration of distribution holes is changed or internal baffles are added at the bottom of the VD as shown in Figure 13 and Figure 14. Different fluidization regimes created by different bottom air distributors under otherwise similar operational conditions, e.g. single bubble and multiple bubble regime, do not have significant effects on the solids concentration profile. The details about the fluidization regimes are discussed in the next section.

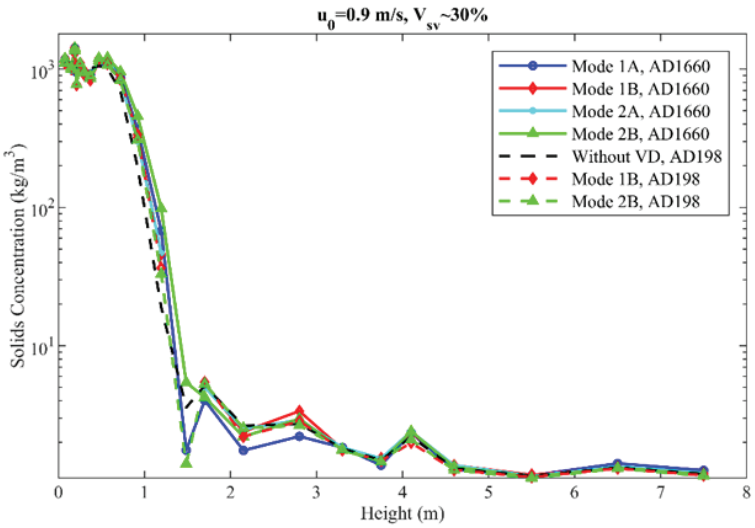

Figure 13. Solids concentration profile along the height of the riser with different AD and VD configurations.

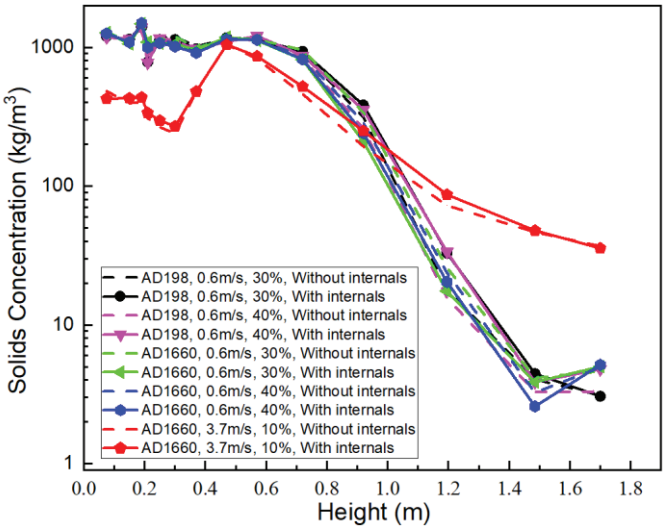

Figure 14. Solids concentration profile at the bottom of the riser with and without internal baffles (VD: Mode 1B).

4.2 Fluidization situation inside the VD

4.2.1 The dense bed inside the VD

The transparent front plate of the riser provides the opportunity to visualize the fluidization in the riser bottom. Figure 15 illustrates the bubble flow under different operational conditions with different VDs and ADs. In the case with AD1660 and without internal baffles, there are big bubbles formed at the bottom when the fluidization velocity is low, which push particles upwards to the top of the VD. When the air distributor is changed to AD198, there are multiple and smaller bubbles formed at the bottom and the dense bed oscillates less violently than in the cases with AD1660.

The dense bed surface becomes more stable by the installation of the internal baffles with the high pressure drop AD198. For the cases with internal baffles under lower fluidization velocities in Figure 15, the internal baffles break the large bubbles, and the movement of particles is reduced by the internal baffles, which helps in creating a more stable dense bed inside the VD.

When the fluidization velocity is increased to 3.7 m/s, the bed inside the VD becomes more diluted and the bed height becomes lower and more unevenly distributed in the lateral direction compared to the lower fluidization velocity cases, as shown in Figure 15 e-f. Note that the inner wall of the VD is also made in perplex, so in the photos with low bed levels, the fluidization behavior of the bed behind, i.e. outside of the VD, can be also seen. There is very little dense bed observed in the case with internal baffles at high fluidization velocity.

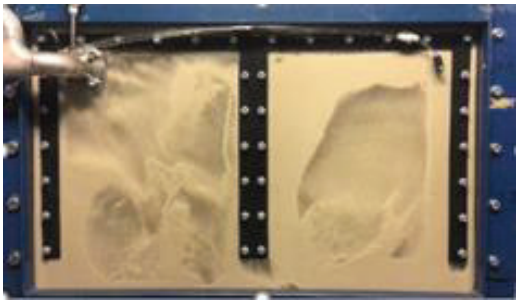

(a) 0.6 m/s, V_{sv}~30%, VD Mode 1B **without** Internal baffles, AD 1660

(b) 0.6 m/s, V_{sv}~30%, VD Mode 1B **with** Internal baffles, AD 1660

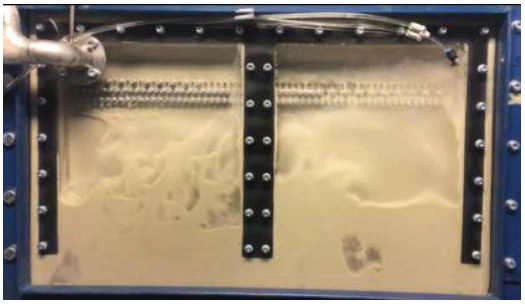

(c) 0.6 m/s, V_{sv}~30%, VD Mode 1B without Internal baffles, AD 198

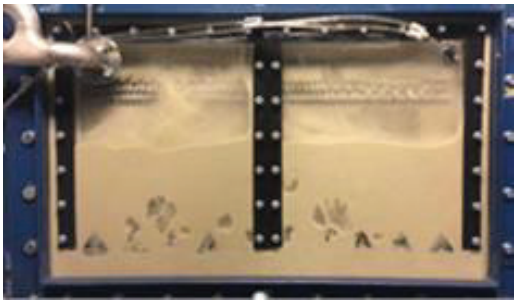

(d) 0.6 m/s, V_{sv}~30%, VD Mode 1B **with** Internal baffles, AD 198

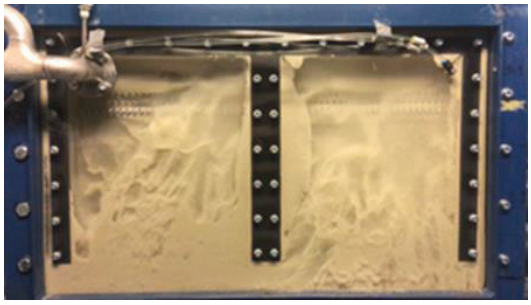

(e) 3.7 m/s, V_{sv}~10%, VD Mode 1B **without** Internal baffles, AD 1660

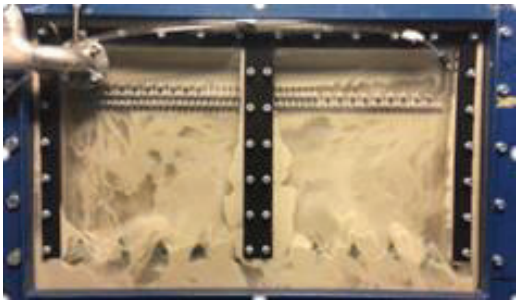

(f) 3.7 m/s, V_{sv}~10%, VD Mode 1B **with** Internal baffles, AD 1660

Figure 15. Captured photos of the bottom riser with different VDs and ADs under different experimental conditions.

4.2.2 Fluidization regime characterization

In this section, an analysis of the pressure fluctuations in the bed and in the wind box is conducted to characterize the fluidization regimes in the riser bottom.

Examples of the pressure behavior are presented in Figure 16. The pressure variations (Figure 16 a-b) show an obvious regularity, which may be caused by large single bubbles (similar to the bubble in Figure 15 a). The frequencies and amplitudes of the pressure variations measured in the wind box and at 0.03 m are similar. This can be illustrated by power spectrum density analysis (Figure 17 a-b). Frequency spectra from the wind box and from the bed both show a sharp peak at somewhat below 1 Hz. This is similar to the results from a previous work done in this experimental system[69]. The sharp peak in the frequency spectrum means a strong periodicity of the formation and eruption of the bubbles, which was characterized as the single bubble regime. In the single bubble regime, most of the bubbles rise up in the center of the bed and the gas flow is discontinuous because of the periodically formed and erupted bubbles. As the fluidization velocity increases from 0.9 m/s to 3.7 m/s, more irregular bubbles (Figure 16 c-d) are formed, which contain more particles compared to the bubbles at lower velocity. i.e. single bubble regime. These irregular bubbles tend to explode at the surface of the bed, and are called exploding bubbles[69]. At the higher velocity, the amplitude of the pressure fluctuation is much lower.

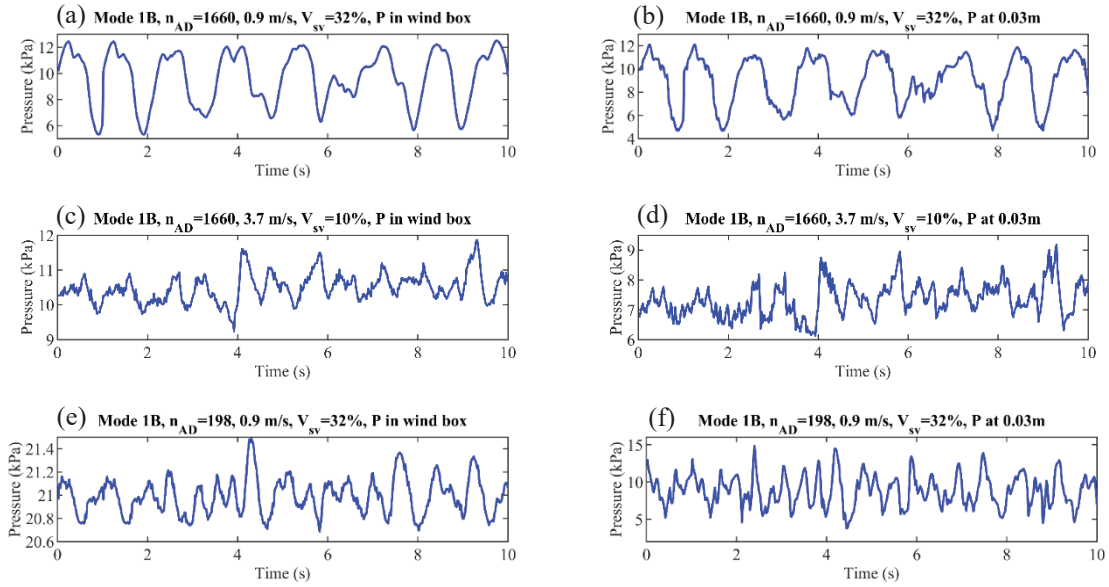

Figure 16. Pressure signal series measured in the wind box and at 0.03 m with VD Mode 1B and different ADs under different operational conditions.

When the air distributor is changed to AD198 from AD1660, the pressure variation periodicity becomes uneven and for AD198 the amplitude differs by a factor higher than

10 between the pressures in the wind box and at 0.03 m (Figure 16 e-f). The pressure vibrates in the range 20.6 ~ 21.5 kPa in the wind box and 4 ~15 kPa at 0.03 m respectively. The multiple and different sizes of bubbles (Figure 15 c) may be the reason for the uneven periodicity. The wide range of frequencies from 1 to 3 Hz in Figure 17 (f) further reflects that there are numerous bubbles with different sizes and formation frequencies in this so-called multiple bubble regime.

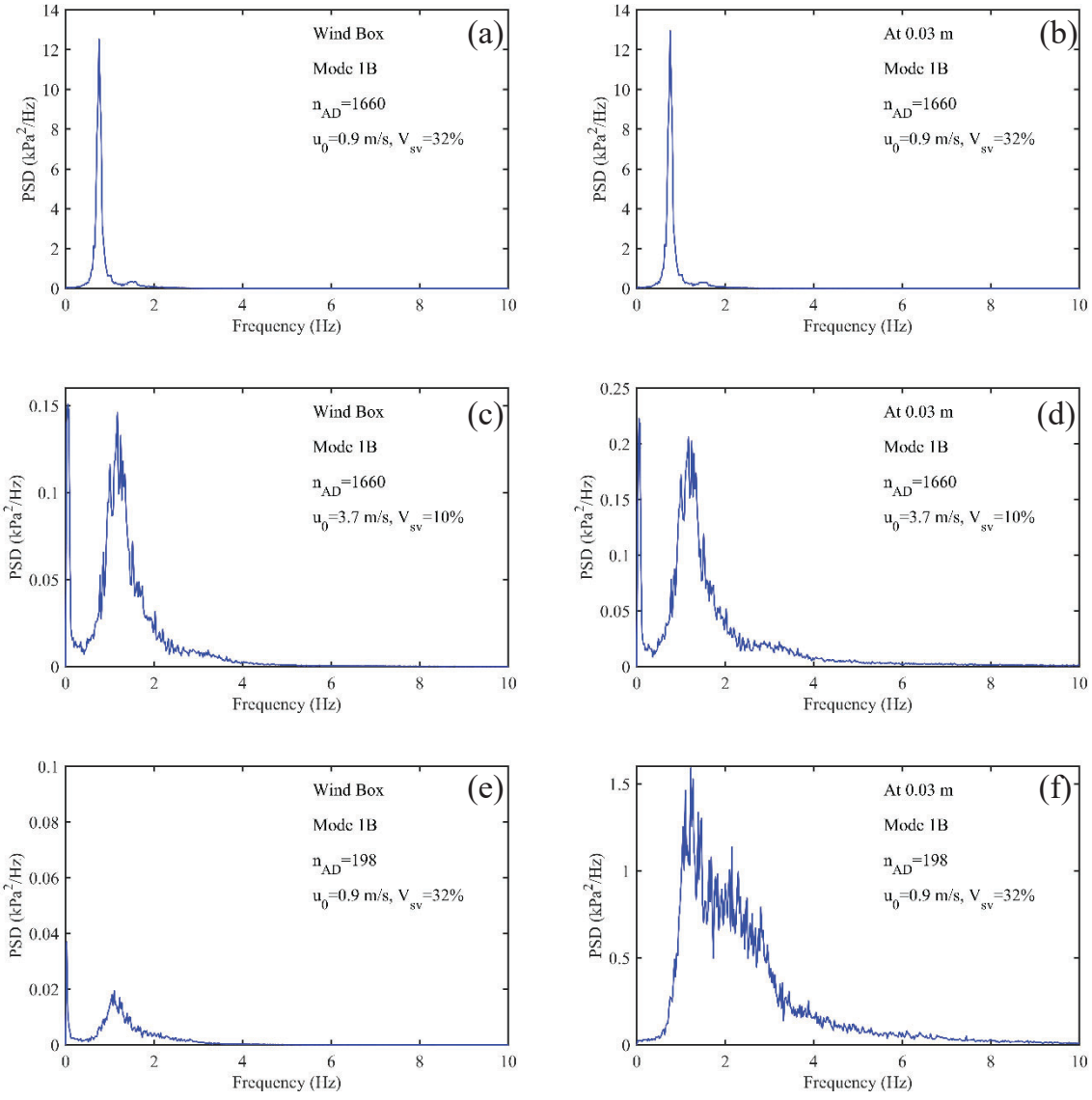

Figure 17. Power spectrum density of the pressure signal in the wind box and in the bed at 0.3 m with different ADs.

The pressure oscillating ranges in the wind box and in the bed are quite similar, i.e. around 7 kPa, under 0.9 m/s fluidization velocity with AD1660. However, they change to around 0.8 kPa and 10 kPa respectively under 0.9 m/s fluidization velocity with AD198. This is caused by the different pressure drops over the air distributor as presented in Table 2, which increases from 0.58 kPa to 11.74 kPa. When the resistance

of the air distributor is low, the local fluidization air flowrate is higher where the pressure right above the distributor is low. For the AD1660 case, the air distributor pressure drop is less than 10% of that of the entire bed. The fluidization air tends to flow continuously into the bubble formed above the air distributor and lead to the large single bubbles formed in AD1660 case.

The correlation between the pressures in the wind box and at 0.03 m in the bed was analyzed based on the CORREL function in excel. The correlation coefficient is used to determine how well the pressures between the wind box and the bed are correlated. Due to the lower pressure drop across the air distributor 1660 compared to AD198, the interaction between the bed and the air supply system is stronger, which can be indicated by the correlation coefficients in Table 2. The correlation coefficients in AD1660 case are close to 1 and those in AD198 case are close to 0, which means the pressures in Figure 16 a and b or c and d are much more correlated than those in Figure 16 e and f. The stronger interaction would be another way to distinguish the exploding bubble regime from the multiple bubble regime, since the multiple bubble regime has lower correlation between the pressure in the wind box and in the bed, and larger difference in frequency spectrum between bed and wind box, as shown in Figure 17.

It is clear that increased pressure drop over the air distributor either by high fluidization velocity or less open area of the air distributor, ensures more uniform distribution of fluidization gas, i.e. wider frequency distribution range.

Table 2. Analysis of pressures over the air distributor and the whole riser.

Parameter		AD1660		AD198	
Fluidization velocity	u_0 [m/s]	0.9	3.7	0.9	0.6
Gauge pressure in the wind box	$p_{windbox}$ [kPa]	9.50	10.43	20.77	14.89
Gauge pressure at the bottom of the riser	p_0 [kPa]	8.92	7.45	9.04	9.34
Gauge pressure at the top of the riser	p_8 [kPa]	0.27	0.89	0.29	0.17
Pressure drop over the air distributor	Δp_{AD} [kPa]	0.58	2.98	11.74	5.55
Pressure drop along the riser	Δp_{riser} [kPa]	8.65	6.56	8.75	9.16
Pressure ratio	$\Delta p_{AD}/\Delta p_{riser}$	7%	45%	134%	61%
Correlation coefficient	-	0.98	0.85	0.21	0.26

4.3 Pressure fluctuations

Figure 18 shows the pressures inside and outside the VD under different fluidization regimes. In general, the average pressure outside the VD is always lower than that inside the VD, which means the dense bed surface inside the VD is always below the level of the distribution holes of the VD. The standard deviation of the pressure outside the VD decreases significantly when the fluidization regime goes from single bubble to multiple

bubble regime, which might be caused by the much smaller bubbles in multiple bubble regime compared to the single bubble regime. However, the standard deviation of the pressure difference over the holes, i.e. P_{in}-P_{out}, in the single bubble regime is lower than that in the multiple bubble regime, which is associated with more correlated pressure fluctuations between inside and outside the VD in the single bubble regime, compared to the multiple bubble regime.

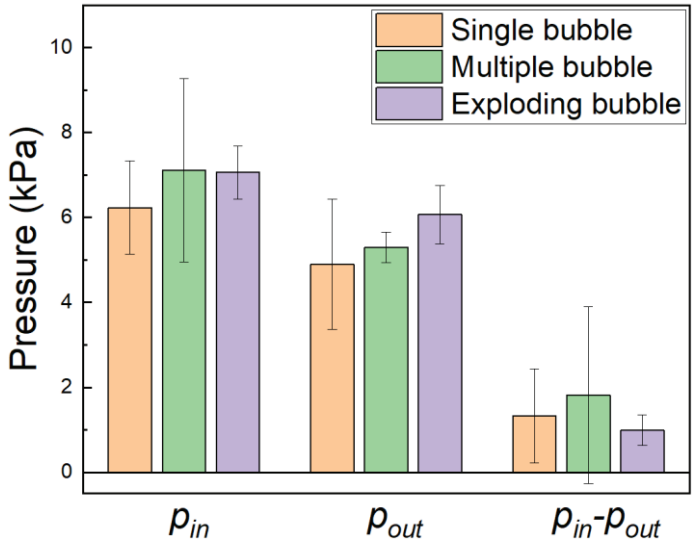

Figure 18. Average pressure and standard deviation of the pressures and pressure drops inside and outside of the VD at the level of the distribution holes under different fluidization regimes.

As Figure 19 shows, the change of the configuration of the holes has no obvious influence on the standard deviations of the pressures. However, as a consequence of doubling the open area of the VD distribution holes, i.e. from Mode 1B to Mode 2B, the pressure difference, i.e. P_{in}-P_{out}, becomes smaller. What's more, the average pressure drop under similar operational conditions with AD1660 doesn't change very much when the VD is changed from Mode 2B to Mode 2A.

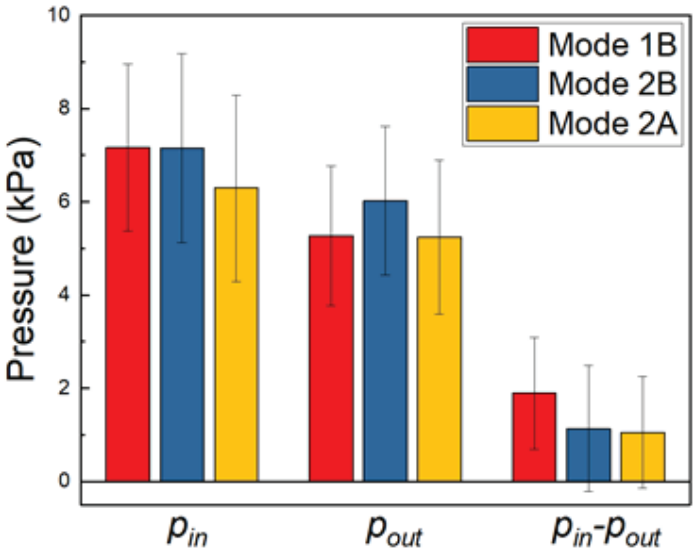

Figure 19. Average pressure and standard deviation of the pressures and pressure drops inside and outside of the VD at the level of the distribution holes with different configurations of distribution holes.

Figure 20 shows the influence of internal baffles on the pressure drops over the distribution holes. Similar decrease of the pressure drop when baffles are added, is found in both the single bubble and multiple bubble regimes, which means less gas passes through the distribution holes with baffles. However, in the exploding bubble regime similar pressure drops over the distribution holes are found with and without internal baffles.

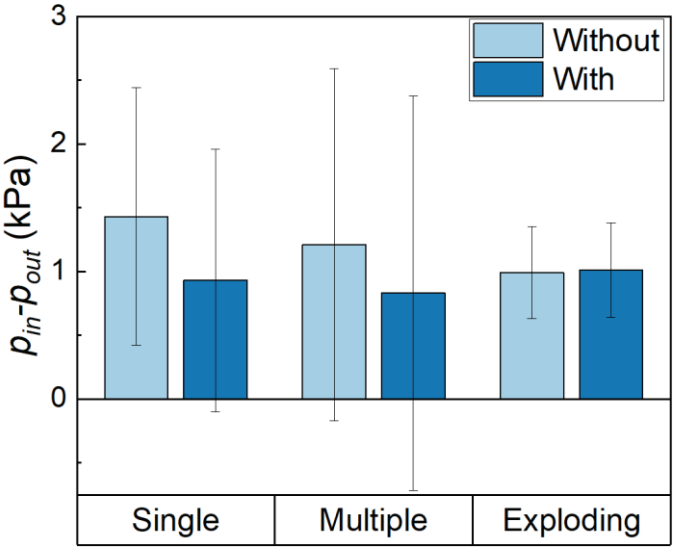

Figure 20. Influence of internal baffles on the average and standard deviation of pressure drop over the distribution holes of the VD under different fluidization regimes. ('Without and with' refer to 'with and without internal baffles')

Less bottom air takes the path through the VD and its distribution holes and more bed material stays inside the VD with the internal baffles present, which gives a higher bed

level inside the VD in both multiple and single bubble regimes as shown in Table 3. However, there is no influence of internal baffles on the dense bed height in the exploding bubble regime. Furthermore, an increased volatiles flow causes higher pressure drop over the distribution holes and lower dense bed level inside the VD.

Table 3 Influence on the dense bed height inside the volatiles distributor.

Air distributor			AD198				AD1660					
Fluidization velocity	u_0	m/s	0.6				0.6				3.7	
Volatiles percentage	$\frac{V_{sv}}{V_{pa}+V_{sv}}$		30%		42%		30%-31%		42%		10%	
Fluidization regime			Multiple bubble				Single bubble				Exploding bubble	
Internal baffles			No baffles	Baffles	No baffles	Baffles	No baffles	Baffles	No baffles	Baffles	No baffles	Baffles
Pressure drop over the VD	$p_{in} - p_{out}$	kPa	1.21	0.83	1.73	1.29	1.43	0.93	1.95	1.37	0.99	1.01
Pressure gradient	dp/dh	kPa/m	10.66	10.56	10.39	10.38	10.73	10.30	10.32	10.13	4.24	4.16
Dense bed height inside VD	h_b	m	0.15	0.18	0.09	0.14	0.13	0.17	0.07	0.12	0.03	0.02

4.4 Horizontal distribution of volatiles

Figure 21 presents the CO_2 ratios at different horizontal positions with VDs of different configurations in the single bubble regime. Generally, the cases with VD have a more even horizontal distribution compared to the experiments without VD. Mode 1B and Mode 2B give a more uniform horizontal distribution at the higher level compared to Mode 1A and 2A. Since the simulated volatiles is injected from the left side, more simulated volatiles would be distributed through the holes near the injection port when the distribution holes are evenly distributed, i.e. Mode 1A and 2A. This is because the gas going through the holes far from the volatiles inlet is more diluted with bottom air entering the VD from below. When the configuration of the distribution holes is uneven, i.e. Mode 1B and Mode 2B, the injected simulated volatiles are forced to flow to the right-hand side giving a more even distribution. Hence, the modified configurations of the VD are helpful in providing a more uniform distribution of the volatiles. There are mainly two sources of the simulated volatiles at the lower level in the riser, i.e. leakage from the bottom of the VD and back mixing near the walls. As Figure 21 shows, there is a large decrease in the CO_2 ratio at LSV1 from Mode 1B to Mode 2B, even though the CO_2 ratio at HSV1 is similar, which indicates that a larger open area of the distribution holes of Mode 2B reduces the bottom leakage of the VD dramatically.

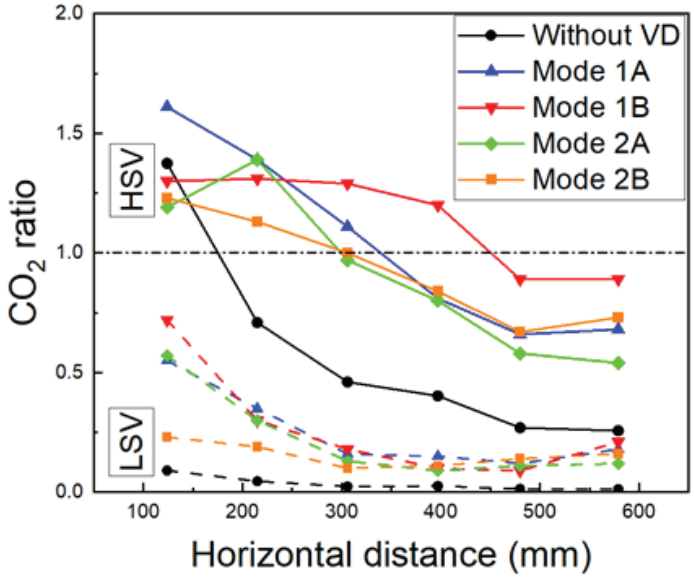

Figure 21. The distribution of volatiles in the horizontal direction from the left to the right side of the riser, with different configurations in single bubble regime. (See Figure 7 for the details of HSV/LSV1-6.)

A comparison between the cases without VD, with VD and with VD equipped with internal baffles in multiple and exploding bubble regime, is shown in Figure 22. It clearly illustrates that the horizontal distribution of volatiles is significantly improved by the VD equipped with internal baffles, especially in multiple bubble regime. The CO_2 ratios keep close to 1 from HSV2 to HSV6 with internal baffles in multiple bubble regime. In the exploding bubble regime, the CO_2 ratio is lowered slightly at the left side and raised at the right side, when using baffles. Thus, the internal baffles fulfil the objective of the uneven holes arrangement, which is to move the volatile gases to the right, i.e. away from the injection port.

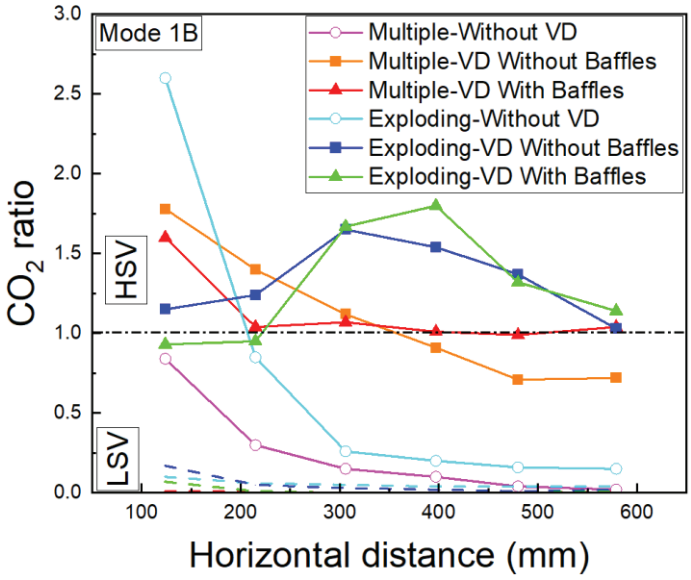

Figure 22. The distribution of volatiles in the horizontal direction from the left to the right side of the riser without VD, with VD and with VD equipped with internal baffles, in multiple and exploding bubble regimes. (See Figure 7 for the details of HSV/LSV1-6.)

4.5 Overall performance of the VD

Table 4 summarizes the results of the experiments with different VD configurations. The standard deviation of the CO_2 ratios at different horizontal positions, together with the relative standard deviation and the ratio between the highest and lowest concentration, gives an overall evaluation on the uniformity of the horizontal distribution of the simulated volatiles by different VDs.

It shows that the VD in Mode 1B and Mode 2B has better overall performances for the horizontal distribution. Furthermore, the SD, RSD and H/L are smallest for the exploding bubble regime (EB), the largest for the multiple bubble regime (MB) and in the middle for the single bubble regime (SB).

Table 4. Statistical evaluation on the performance of different VDs under different experimental conditions. *SD*: standard deviation, *RSD*: relative standard deviation, *H/L*: highest/lowest concentration.

Air distributor	VD holes arrangement	Fluidization velocity/Regime $u_0\ [m/s]$	Simulated volatiles percentage V_{sv}	Open area of the VD $A\ [m^2]$	Average CO_2 ratio	*SD*	*RSD*	*H/L*
AD1660	Mode 1A	0.9/SB	7%	1.138×10^{-3}	1.21	0.57	47%	3.5
			30%		1.01	0.36	36%	2.51
		3.7/EB	10%		1.07	0.25	23%	1.86
	Mode 1B	0.9/SB	10%		1.44	0.55	38%	2.69
			32%		1.14	0.18	16%	1.48
		3.7/EB	10%		1.31	0.2	16%	1.58
	Mode 2A	0.9/SB	11%	2.276×10^{-3}	1.25	0.73	59%	4.86
			32%		1.01	0.48	48%	3.64
		3.7/EB	10%		1.3	0.59	45%	4.81
	Mode 2B	0.9/SB	11%		0.95	0.28	29%	2.14
			32%		0.92	0.21	22%	1.85
		3.7/EB	10%		1.14	0.31	28%	2.13
AD198	Mode 1B	0.9/MB	32%	1.138×10^{-3}	1.16	0.42	36%	2.56
		0.6/MB	30%		1.12	0.39	35%	2.52
			42%		1.02	0.29	28%	2.2
	Mode 2B	0.9/MB	33%	2.276×10^{-3}	0.95	0.39	42%	2.95
		0.6/MB	30%		0.97	0.53	55%	4.38
			43%		0.94	0.36	38%	2.72

Table 5 shows the overall performance of the VD with and without internal baffles under different operational conditions. In the multiple and single bubble regimes, the standard deviation, and relative standard deviation of the CO_2 ratios, together with the highest/lowest concentration, are much lower in the cases with internal baffles.

In the exploding bubble regime, the standard deviation, the relative standard deviation and the highest/lowest concentration of CO_2 ratios are higher in the case with internal baffles compared to the case without baffles. This can be explained by lower CO_2 ratios at HSV1 and HSV2 and higher ones at HSV4 and HSV5 in the case with internal baffles compared to the case without baffles, which means that the installation of the internal baffles help the VD push more simulated volatiles to be distributed from the side further away from the simulated volatiles injection port. Thus, the internal baffles do not improve the distribution of the simulated volatiles in the exploding bubble regime, but it does amplify the movement of volatiles away from the injection port, which is the purpose of the uneven hole distribution. This means that the internal baffles facilitate the control over the distribution, which is an important point considering the application in longer VD arms.

Table 5. General performance of the VD with and without internal baffles under different operation conditions.

Air distributor	Fluidization velocity	Fluidization regime	Simulated volatiles percentage	Average CO_2 ratio		*SD*		*RSD*		*H/L*	
	m/s			No baffles	Baffles	No baffles	Baffles	No baffles	Baffles	No baffles	Baffles
AD198	0.6	Multiple bubble	30%	1.11	1.13	0.38	0.21	0.35	0.19	2.52	1.61
			42%	1.00	1.05	0.29	0.12	0.29	0.11	2.20	1.39
AD1660		Single bubble	30-31%	1.20	1.22	0.41	0.19	0.34	0.16	2.30	1.55
			42%	1.06	1.21	0.23	0.18	0.22	0.15	1.80	1.51
	3.7	Exploding bubble	10%	1.33	1.30	0.21	0.34	0.16	0.26	1.60	1.95

It is shown in Table 5 that the standard deviation, relative standard deviation, and the highest/lowest concentration are much lower when the volatiles percentage increases in the single and multiple bubble regime for the reference cases without internal baffles. However, these values remain similar in the cases with internal baffles, especially in the single bubble regime, which means that once the internal baffles are installed, the flowrate of simulated volatiles would not have a big impact on the horizontal distribution by the VD.

Generally, the VDs with less open area or internal baffles at bottom give a better horizontal tracer distribution across the cross section by comparing the values of SD, RSD and c_H/c_L in Table 4 and Table 5.

4.6 Dilution of volatiles inside the VD

Table 6 presents the calculation results of the simulated volatiles dilution inside the VD according to the orifice discharge coefficient equation. Dilution of volatiles inside the VD was analyzed based on the dilution factors i.e. V_{ba}/V_{sv} and c_{vd}/c_{sv}.

The volatiles injected into the VD are diluted by the bottom air flowing into the VD. When internal baffles are installed in the VD, as shown in Table 6 there is less bottom air flowing into the VD and the dilution of the injected simulated volatiles is smaller, especially in the single and multiple bubble regime. The lower dilution results in more even distribution of the volatiles. However, there is no big difference in the volatiles dilution inside the VD in the exploding bubble regime, i.e. the degree of bottom air flow coming into the VD before and after the installation of the internal baffles is largely the same.

Table 6. Volatiles dilution inside the VD estimated based on orifice discharge coefficient.

Air distributor	Fluidization velocity	Fluidization regime	Volatiles percentage	Internal Baffle	$p_{in} - p_{out}$	Gas velocity through orifices	Gas flow from the bottom of VD	Fluidization velocity inside VD	CO_2 concentration inside VD	Dilution Factors	
					kPa	$v_{orifice}$ m/s	V_{ba} m_n^3/h	u_{VD} m/s	c_{vd} ppm	$\frac{V_{ba}}{V_{sv}}$	$\frac{c_{vd}}{c_{sv}}$
AD198	0.6 m/s	Multiple bubble	30%	No	1.21	41.52	100	1.17	4934	1.43	0.44
				Yes	0.83	34.44	70	0.82	8267	0.98	0.76
			40%	No	1.73	49.61	81	0.95	10365	0.66	0.70
				Yes	1.29	42.91	53	0.62	10327	0.43	0.92
AD1660	0.6 m/s	Single bubble	30%	No	1.43	45.20	115	1.34	5829	1.62	0.53
				Yes	0.93	36.42	76	0.89	8421	1.03	0.79
			40%	No	1.95	52.73	98	1.15	7558	0.84	0.67
				Yes	1.37	44.13	57	0.67	9213	0.46	0.90
	3.7 m/s	Exploding bubble	10%	No	0.99	37.49	43	0.50	9123	0.39	0.75
				Yes	1.01	37.92	45	0.53	8578	0.41	0.79

4.7 Implications for large-scale application of the VD

The investigation of the VD has been made in a cold-flow fluidized-bed model under varying fluidization regimes. The performance of the VD in the cold-flow model gives some hints for the performance of the VD in a real-world application with the same fluidization regime. But, what would be the expected operational conditions in a future fuel reactor using solid fuels? There are some differences between the operational conditions in current investigations in the cold-flow model and the ones in the large-scale fuel reactors.

Firstly, the bottom fluidization gas flow would be low in a real-world fuel reactor. The bottom gas, either steam or a combination of steam and recycled CO_2, comes with a significant cost, and its major purpose is to keep the bed fluidized. Thus, the optimal bottom gas flow is likely the minimum flow needed to safely achieve adequate fluidizing conditions. Apart from the bottom fluidization gas flow, there are two major gas flows in the fuel reactor originating from the char and the volatiles. The char will mainly be part of the dense phase. Thus, the syngas produced by gasification will also appear in the dense phase. This will make the dense phase “self-fluidizing”, which is likely helpful for improving the gas-solid contacting. It also means that the gas flow in the dense phase outside the VD will increase with bed height. Such a “self-fluidizing” regime is obviously difficult to accomplish in a cold-flow model. Therefore, it is

relevant to consider different fluidization velocities in the evaluation, i.e. from the low velocities, typical of the fluidization flow, to the higher flows which are more relevant higher up in the bed. A second difference is that the flow of volatiles in a fuel reactor which uses a highly volatile biomass fuel, would be significantly higher than that used in these tests, because of practical limitations to the flow of simulated volatiles that could be added. A higher flow would obviously have implications for the dimensioning of the arms and the open area of the holes.

Despite these differences, it can nevertheless be concluded that the concept has been proven and can be expected to be useful in real-world applications. Moreover, the different configurations and conditions examined in this work should be helpful in the designing of large-scale applications.

CHAPTER 5

5 Conclusion

In this thesis the concept of a volatiles distributor, has been proposed and studied experimentally in a cold-flow fluidized-bed model. The aim is to achieve a more even cross-sectional distribution of volatiles, provide better gas-solid contacting and improve the gas conversion in the fuel reactor. The performance of the volatiles distributor has been evaluated based on the results of the pressure and tracer gas concentration measurements under different operational conditions, i.e. different fluidization velocities and simulated volatiles flow, with volatiles distributors and air distributors of different configurations.

The gas-solid contacting and the performance of the VD depend on the fluidization regime. Further, the fluidization regime is dependent on the fluidization velocity, but also on the air distributors leading the fluidization gas into the bottom bed. The single bubble regime, i.e. large single bubbles formed at the bottom, exploding bubble regime, i.e. irregular bubbles containing more particles, and multiple bubble regime, i.e. multiple bubbles with different sizes formed at the bottom, were investigated with the VD. It was found that the horizontal distribution of volatiles could be improved significantly by the VD, especially in exploding bubble regime. Higher flowrate of simulated volatiles increases the pressure drop over the distribution holes, lowers the bed level inside the VD and thus improves the uniformity of horizontal distribution of volatiles to some extent.

The configurations of the VD investigated, have different numbers of distribution holes and different holes arrangements, including evenly and unevenly distributed holes. The latter involves less holes close to the entrance of volatiles and more holes at the far end.

It was found that the arrangement with unevenly distributed holes can improve the uniformity of the horizontal distribution of volatiles. Less open area of the distribution holes in the VD increases the pressure drop over the distribution holes and also increases the risk of volatiles slip below the lower edge of the VD, in particular in the single bubble regime.

The installation of internal baffles at the bottom of the VD was found to reduce the pressure drop over the distribution holes, and make more particles stay inside the VD and lower the upward flow of bottom air inside the VD in both single and multiple bubble regime; thus improving the uniformity of the horizontal distribution of the volatiles and reducing the risk of volatiles slip below the lower edge of the VD close to the volatiles inlet. Also in the exploding bubble regime the baffles promoted a shift of volatiles away from the inlet.

In general, the effectiveness of the concept of the VD has been proven and the flexibility of the design of the VD has also been demonstrated in the cold-flow model, with different configurations, i.e. different open area of the distribution holes and different holes arrangements, and internal baffles at the bottom of the VD. These flexibilities of the design should be important and instructive for the large-scale applications of the volatiles distributor.

Nomenclature

ABBREVIATIONS

AD198	Air distributor with 198 holes
AD1660	Air distributor with 1660 holes
BECCS	Bioenergy carbon capture and storage
Bio-CLC	Chemical looping combustion of biomass
CLC	Chemical looping combustion
CLOU	Chemical looping with oxygen uncoupling
EB	Exploding bubble regime
FFT	Fast Fourier transform
GHG	Greenhouse gas
HSV	High-level sampled volatiles
IPCC	Intergovernmental Panel on Climate Change
LSV	Low-level sampled volatiles
MB	Multiple bubble regime
OC	Oxygen carriers
PSD	Power spectral density
RSD	Relative standard deviation
SB	Single bubble regime
SD	Standard deviation
VD	Volatiles distributor

NOTATIONS

$A_{orifice}$	Open area of the orifices [m^2]
c_{cal}	Ideal average CO_2 concentration in the cross-section of the riser [ppm]
c_m	Measured CO_2 concentration [ppm]
$c_{s,h_{1\to2}}$	Solids concentration in the middle of h_1 and h_2 [kg/m^3]
$c_{VD,mea}$	CO_2 concentration measured inside VD [ppm]
$c_{VD,avg}$	Average CO_2 concentration inside VD [ppm]
$\bar{c}$	Average CO_2 ratio [$-$]
c_H/c_L	Ratio between the highest and the lowest CO_2 concentration at HSV [$-$]
C_d	Orifice discharge coefficient [$-$]
D_1, D_2	Dilution factors of the concentration inside the VD [$-$]
dp/dh	Pressure drop gradient [kPa/m]
f_s	Pressure sampling frequency [Hz]
Δf	Frequency resolution [Hz]
$F(f)$	Fourier transform of the autocorrelation sequence of the time series of pressure signals [kPa]
g	Acceleration of gravity [m/s^2]
h_1, h_2	Different heights of the pressure measurement positions [m]
h_b	Dense bed height inside volatiles distributor [m]
h_{bottom}	Height of the bottom of the volatiles distributor [m]
h_{hole}	Height of the distribution holes [m]
Δh	Distance between the dense bed height inside the VD and the distribution holes level [m]
L	Number of pressure signals segments [$-$]
MF_{CO_2}	CO_2 flow [m_n^3/h]
MF_{SA}	Air flow used for simulating volatiles [m_n^3/h]

MF_{PA}	Primary air flow for the main fluidization $[m_n^3/\mathrm{h}]$
N_s	Length of segments of the pressure signals $[-]$
$P_{xx}(f)$	Power spectrum density $[kPa^2/Hz]$
$p_{windbox}$	Pressure inside the wind box $[kPa]$
p_0	Pressure at the bottom of the riser $[kPa]$
p_8	Pressure at the top of the riser $[kPa]$
Δp_{AD}	Pressure drop over the air distributor $[kPa]$
Δp_{riser}	Pressure drop along the riser $[kPa]$
p_{h_1}, p_{h_2}	Pressures measured at height h_1 and h_2 $[kPa]$
p_{in}	Pressure inside the VD measured at the top right corner $[kPa]$
p_{out}	Pressure outside the VD measured at the back side of the riser at the distribution holes level $[kPa]$
$\bar{p}$	Average pressure $[kPa]$
T	Plate thickness $[mm]$
L_h	Hole pitch $[mm]$
u_0	Fluidization velocity $[m/s]$
u_{VD}, u'_{VD}	Fluidization velocity inside the VD based on two calculation methods $[m/s]$
v	Orifice velocity $[m/s]$
V_{ba}	Bottom air flow from the main riser to the VD $[m_n^3/\mathrm{h}]$
V_{CO_2}	CO_2 flowrate $[m_n^3/\mathrm{h}]$
V_{pa}	Primary air flowrate $[m_n^3/\mathrm{h}]$
V_{sv}	Simulated volatiles flowrate $[m_n^3/\mathrm{h}]$
$V_{orifice}$	Orifice gas flow $[m_n^3/\mathrm{h}]$
$x_i(n)$	Time series of pressure signals $[kPa]$
ρ_{gas}	Density of gas (air) $[\mathrm{kg/m^3}]$

ρ_s	Density of bed materials $[\mathrm{kg/m^3}]$
σ	Standard deviation of pressures $[kPa]$

Reference

[1] V. Masson-Delmotte, P. Zhai, A. Pirani, S.L. Connors, C. Péan, S. Berger, N. Caud, Y. Chen, L. Goldfarb, M.I. Gomis, M. Huang, K. Leitzell, E. Lonnoy, J.B.R. Matthews, T.K. Maycock, T. Waterfield, O. Yelekçi, R. Yu, B.Z. (eds.), IPCC, 2021: Summary for Policymakers. In: Climate Change 2021: The Physical Science Basis. Contribution of Working Group I to the Sixth Assessment Report of the Intergovernmental Panel on Climate Change, Cambridge University Press, In Press.
[2] V. Masson-Delmotte, P. Zhai, H.-O. Pörtner, IPCC, 2018: Summary for Policymakers. In: Global warming of 1.5°C. An IPCC Special Report on the impacts of global warming of 1.5°C above pre-industrial levels and related global greenhouse gas emission pathways, in the context of strengthening the global response to the threat of climate change, sustainable development, and efforts to eradicate poverty, In Press, (2018).
[3] S. Fuss, W. Lamb, M. Callaghan, J. Hilaire, F. Creutzig, T. Amann, T. Beringer, W. de Oliveira Garcia, J. Hartmann, T. Khanna, G. Luderer, G. Nemet, J. Rogelj, P. Smith, J. Vicente Vicente, J. Wilcox, M. Dominguez, J. Minx, Negative emissions—Part 2: Costs, potentials and side effects, Environmental Research Letters, 13 (2018) 063002.
[4] M. Rydén, A. Lyngfelt, Ø. Langørgen, Y. Larring, A. Brink, S. Teir, H. Havåg, P. Karmhagen, Negative CO2 Emissions with Chemical-Looping Combustion of Biomass – A Nordic Energy Research Flagship Project, Energy Procedia, 114 (2017) 6074-6082.
[5] A. Lyngfelt, B. Leckner, A 1000 MWth boiler for chemical-looping combustion of solid fuels – Discussion of design and costs, Applied Energy, 157 (2015) 475-487.
[6] C. Linderholm, A. Lyngfelt, A. Cuadrat, E. Jerndal, Chemical-looping combustion of solid fuels – Operation in a 10 kW unit with two fuels, above-bed and in-bed fuel feed and two oxygen carriers, manganese ore and ilmenite, Fuel, 102 (2012) 808-822.
[7] A. Lyngfelt, Chemical Looping Combustion: Status and Development Challenges, Energy & Fuels, 34 (2020) 9077-9093.
[8] M. Kramp, A. Thon, E.-U. Hartge, S. Heinrich, J. Werther, Carbon Stripping – A Critical Process Step in Chemical Looping Combustion of Solid Fuels, Chemical Engineering & Technology, 35 (2012) 497-507.
[9] H. Sun, M. Cheng, D. Chen, L. Xu, Z. Li, N. Cai, Experimental Study of a Carbon Stripper in Solid Fuel Chemical Looping Combustion, Industrial & Engineering Chemistry Research, 54 (2015) 8743-8753.
[10] H. Sun, M. Cheng, Z. Li, N. Cai, Riser-Based Carbon Stripper for Coal-Fueled Chemical Looping Combustion, Industrial & Engineering Chemistry Research, 55 (2016) 2381-2390.
[11] N. Berguerand, A. Lyngfelt, Design and operation of a 10 kWth chemical-looping combustor for solid fuels – Testing with South African coal, Fuel, 87 (2008) 2713-2726.
[12] C. Linderholm, M. Schmitz, P. Knutsson, M. Källén, A. Lyngfelt, Use of Low-Volatile Solid Fuels in a 100 kW Chemical-Looping Combustor, Energy & Fuels, 28 (2014) 5942-5952.

[13] H. Chen, M. Cheng, L. Liu, Y. Li, Z. Li, N. Cai, Coal-fired chemical looping combustion coupled with a high-efficiency annular carbon stripper, International Journal of Greenhouse Gas Control, 93 (2020) 102889.
[14] I. Gogolev, A.H. Soleimanisalim, C. Linderholm, A. Lyngfelt, Commissioning, performance benchmarking, and investigation of alkali emissions in a 10 kWth solid fuel chemical looping combustion pilot, Fuel, 287 (2021) 119530.
[15] A. Lyngfelt, C. Linderholm, Chemical-Looping Combustion of Solid Fuels – Status and Recent Progress, Energy Procedia, 114 (2017) 371-386.
[16] J. Ströhle, M. Orth, B. Epple, Chemical looping combustion of hard coal in a 1MWth pilot plant using ilmenite as oxygen carrier, Applied Energy, 157 (2015) 288-294.
[17] T. Berdugo Vilches, F. Lind, M. Rydén, H. Thunman, Experience of more than 1000h of operation with oxygen carriers and solid biomass at large scale, Applied Energy, 190 (2017) 1174-1183.
[18] I. Petersen, J. Werther, Three-dimensional modeling of a circulating fluidized bed gasifier for sewage sludge, Chemical Engineering Science, 60 (2005) 4469-4484.
[19] D. Mei, C. Linderholm, A. Lyngfelt, Performance of an oxy-polishing step in the 100 kWth chemical looping combustion prototype, Chemical Engineering Journal, 409 (2021) 128202.
[20] H. Gu, L. Shen, J. Xiao, S. Zhang, T. Song, Chemical Looping Combustion of Biomass/Coal with Natural Iron Ore as Oxygen Carrier in a Continuous Reactor, Energy & Fuels, 25 (2011) 446-455.
[21] T. Mendiara, A. Abad, L.F. de Diego, F. García-Labiano, P. Gayán, J. Adánez, Biomass combustion in a CLC system using an iron ore as an oxygen carrier, International Journal of Greenhouse Gas Control, 19 (2013) 322-330.
[22] F. Miccio, A. Natali Murri, E. Landi, Synthesis and characterization of geopolymer oxygen carriers for chemical looping combustion, Applied Energy, 194 (2017) 136-147.
[23] C. Linderholm, M. Schmitz, P. Knutsson, A. Lyngfelt, Chemical-looping combustion in a 100-kW unit using a mixture of ilmenite and manganese ore as oxygen carrier, Fuel, 166 (2016) 533-542.
[24] J. Wang, H. Zhao, Evaluation of CaO-decorated Fe2O3/Al2O3 as an oxygen carrier for in-situ gasification chemical looping combustion of plastic wastes, Fuel, 165 (2016) 235-243.
[25] A. Lyngfelt, A. Brink, Ø. Langørgen, T. Mattisson, M. Rydén, C. Linderholm, 11,000 h of chemical-looping combustion operation—Where are we and where do we want to go?, International Journal of Greenhouse Gas Control, 88 (2019) 38-56.
[26] T. Mendiara, L.F. de Diego, F. García-Labiano, P. Gayán, A. Abad, J. Adánez, On the use of a highly reactive iron ore in Chemical Looping Combustion of different coals, Fuel, 126 (2014) 239-249.
[27] M. Schmitz, C. Linderholm, Chemical looping combustion of biomass in 10- and 100-kW pilots – Analysis of conversion and lifetime using a sintered manganese ore, Fuel, 231 (2018) 73-84.
[28] T. Mendiara, L.F. de Diego, F. García-Labiano, P. Gayán, A. Abad, J. Adánez, Behaviour of a bauxite waste material as oxygen carrier in a 500Wth CLC unit with coal, International Journal of Greenhouse Gas Control, 17 (2013) 170-182.

[29] J. Haus, K. Lyu, E.-U. Hartge, S. Heinrich, J. Werther, Analysis of a Two-Stage Fuel Reactor System for the Chemical-Looping Combustion of Lignite and Bituminous Coal, Energy Technology, 4 (2016) 1263-1273.
[30] M. Schmitz, C.J. Linderholm, A. Lyngfelt, Chemical looping combustion of four different solid fuels using a manganese-silicon-titanium oxygen carrier, International Journal of Greenhouse Gas Control, 70 (2018) 88-96.
[31] R. Pérez-Vega, A. Abad, F. García-Labiano, P. Gayán, L.F. de Diego, M.T. Izquierdo, J. Adánez, Chemical Looping Combustion of gaseous and solid fuels with manganese-iron mixed oxide as oxygen carrier, Energy Conversion and Management, 159 (2018) 221-231.
[32] T. Mattisson, A. Lyngfelt, H. Leion, Chemical-looping with oxygen uncoupling for combustion of solid fuels, International Journal of Greenhouse Gas Control, 3 (2009) 11-19.
[33] H. Leion, T. Mattisson, A. Lyngfelt, Using chemical-looping with oxygen uncoupling (CLOU) for combustion of six different solid fuels, Energy Procedia, 1 (2009) 447-453.
[34] M. Arjmand, A.-M. Azad, H. Leion, A. Lyngfelt, T. Mattisson, Prospects of Al_2O_3 and $MgAl_2O_4$-Supported CuO Oxygen Carriers in Chemical-Looping Combustion (CLC) and Chemical-Looping with Oxygen Uncoupling (CLOU), Energy & Fuels, 25 (2011) 5493-5502.
[35] P. Gayán, I. Adánez-Rubio, A. Abad, L.F. de Diego, F. García-Labiano, J. Adánez, Development of Cu-based oxygen carriers for Chemical-Looping with Oxygen Uncoupling (CLOU) process, Fuel, 96 (2012) 226-238.
[36] M. Arjmand, M. Keller, H. Leion, T. Mattisson, A. Lyngfelt, Oxygen Release and Oxidation Rates of $MgAl_2O_4$-Supported CuO Oxygen Carrier for Chemical-Looping Combustion with Oxygen Uncoupling (CLOU), Energy & Fuels, 26 (2012) 6528-6539.
[37] A. Shulman, E. Cleverstam, T. Mattisson, A. Lyngfelt, Manganese/Iron, Manganese/Nickel, and Manganese/Silicon Oxides Used in Chemical-Looping With Oxygen Uncoupling (CLOU) for Combustion of Methane, Energy & Fuels, 23 (2009) 5269-5275.
[38] G. Azimi, H. Leion, T. Mattisson, A. Lyngfelt, Chemical-looping with oxygen uncoupling using combined Mn-Fe oxides, testing in batch fluidized bed, Energy Procedia, 4 (2011) 370-377.
[39] G. Azimi, H. Leion, M. Rydén, T. Mattisson, A. Lyngfelt, Investigation of Different Mn–Fe Oxides as Oxygen Carrier for Chemical-Looping with Oxygen Uncoupling (CLOU), Energy & Fuels, 27 (2013) 367-377.
[40] A. Natali Murri, F. Miccio, V. Medri, E. Landi, Geopolymer-composites with thermomechanical stability as oxygen carriers for fluidized bed chemical looping combustion with oxygen uncoupling, Chemical Engineering Journal, 393 (2020) 124756.
[41] I. Adánez-Rubio, A. Abad, P. Gayán, L.F. de Diego, J. Adánez, CLOU process performance with a Cu-Mn oxygen carrier in the combustion of different types of coal with CO2 capture, Fuel, 212 (2018) 605-612.
[42] T. Mendiara, I. Adánez-Rubio, P. Gayán, A. Abad, L.F. de Diego, F. García-Labiano, J. Adánez, Process Comparison for Biomass Combustion: In Situ

Gasification-Chemical Looping Combustion (iG-CLC) versus Chemical Looping with Oxygen Uncoupling (CLOU), Energy Technology, 4 (2016) 1130-1136.
[43] E.R. Stobbe, B.A. de Boer, J.W. Geus, The reduction and oxidation behaviour of manganese oxides, Catalysis Today, 47 (1999) 161-167.
[44] P. Moldenhauer, M. Rydén, T. Mattisson, A. Lyngfelt, Chemical-looping combustion and chemical-looping with oxygen uncoupling of kerosene with Mn- and Cu-based oxygen carriers in a circulating fluidized-bed 300W laboratory reactor, Fuel Processing Technology, 104 (2012) 378-389.
[45] I. Adánez-Rubio, P. Gayán, A. Abad, L.F. de Diego, F. García-Labiano, J. Adánez, Evaluation of a Spray-Dried $CuO/MgAl_2O_4$ Oxygen Carrier for the Chemical Looping with Oxygen Uncoupling Process, Energy & Fuels, 26 (2012) 3069-3081.
[46] C. Kuang, S. Wang, M. Luo, J. Cai, J. Zhao, Investigation of CuO-based oxygen carriers modified by three different ores in chemical looping combustion with solid fuels, Renewable Energy, 154 (2020) 937-948.
[47] J. Dai, K.J. Whitty, Impact of fuel-derived chlorine on CuO-based oxygen carriers for chemical looping with oxygen uncoupling, Fuel, 263 (2020) 116780.
[48] J. Yan, L. Shen, S. Jiang, J. Wu, T. Shen, T. Song, Combustion Performance of Sewage Sludge in a Novel CLC System with a Two-Stage Fuel Reactor, Energy & Fuels, 31 (2017) 12570-12581.
[49] D. Kunii, O. Levenspiel, CHAPTER 9 - Solid Movement: Mixing, Segregation, and Staging, in: D. Kunii, O. Levenspiel (Eds.) Fluidization Engineering (Second Edition), Butterworth-Heinemann, Boston, 1991, pp. 211-235.
[50] L. Massimilla, H.F. Johnstone, Reaction kinetics in fluidized beds, Chemical Engineering Science, 16 (1961) 105-112.
[51] D.C. Guío-Pérez, T. Pröll, H. Hofbauer, Influence of ring-type internals on the solids residence time distribution in the fuel reactor of a dual circulating fluidized bed system for chemical looping combustion, Chemical Engineering Research and Design, 92 (2014) 1107-1118.
[52] R. Pérez-Vega, A. Abad, J.A. Bueno, F. García-Labiano, P. Gayán, L.F. de Diego, J. Adánez, Improving the efficiency of Chemical Looping Combustion with coal by using ring-type internals in the fuel reactor, Fuel, 250 (2019) 8-16.
[53] T. Song, L. Shen, Review of reactor for chemical looping combustion of solid fuels, International Journal of Greenhouse Gas Control, 76 (2018) 92-110.
[54] A. Cuadrat, A. Abad, F. García-Labiano, P. Gayán, L.F. de Diego, J. Adánez, The use of ilmenite as oxygen-carrier in a 500Wth Chemical-Looping Coal Combustion unit, International Journal of Greenhouse Gas Control, 5 (2011) 1630-1642.
[55] A. Abad, I. Adánez-Rubio, P. Gayán, F. García-Labiano, L.F. de Diego, J. Adánez, Demonstration of chemical-looping with oxygen uncoupling (CLOU) process in a 1.5kWth continuously operating unit using a Cu-based oxygen-carrier, International Journal of Greenhouse Gas Control, 6 (2012) 189-200.
[56] T. Sozinho, W. Pelletant, T. Gauthier, H. Stainton, Main results of the 10 kW coal pilot plant operation, in: 2nd Int. Conf. on Chemical Looping, 2012.
[57] A. Thon, M. Kramp, E.-U. Hartge, S. Heinrich, J. Werther, Operational experience with a system of coupled fluidized beds for chemical looping combustion of solid fuels using ilmenite as oxygen carrier, Applied Energy, 118 (2014) 309-317.

[58] F. Mayer, A. Bidwe, A. Schopf, K. Taheri, M. Zieba, G. Scheffknecht, Comparison of a new micaceous iron oxide and ilmenite with respect to syngas conversion in a BFB reactor and adaptation of a 10 kWth DFB system for CLC to solid fuels, in: 2nd International Conference on Chemical Looping. Darmstadt (Germany), 2012.
[59] J. Ma, H. Zhao, P. Niu, X. Chen, X. Tian, C. Zheng, Design and operation of a 50 kWth chemical looping combustion (CLC) reactor using coal as fuel, in: Proceedings of the 4th International Conference on Chemical Looping, Southeast University, Nanjing, China, 2016, pp. 26-28.
[60] T. Pikkarainen, I. Hiltunen, S. Teir, Piloting of bio-CLC for BECCS, in: 4th International Conference on Chemical Looping, 2016.
[61] I. Abdulally, C. Beal, H. Andrus, B. Epple, A. Lyngfelt, B. Lani, Alstom's chemical looping prototypes, program update, in: 37th International technical conference on clean coal & fuel systems, 2012, pp. 3-7.
[62] P. Markström, A. Lyngfelt, Designing and operating a cold-flow model of a 100kW chemical-looping combustor, Powder Technology, 222 (2012) 182-192.
[63] M. Orth, J. Ströhle, B. Epple, Design and operation of a 1 MWth chemical looping plant, in: Proceedings from the 2nd International Conference on Chemical Looping, 2012, pp. 26-28.
[64] R. Xiao, L. Chen, C. Saha, S. Zhang, S. Bhattacharya, Pressurized chemical-looping combustion of coal using an iron ore as oxygen carrier in a pilot-scale unit, International Journal of Greenhouse Gas Control, 10 (2012) 363-373.
[65] J. Adánez, A. Abad, R. Perez-Vega, L.F. de Diego, F. García-Labiano, P. Gayán, Design and Operation of a Coal-fired 50 kWth Chemical Looping Combustor, Energy Procedia, 63 (2014) 63-72.
[66] J. Ma, H. Zhao, X. Tian, Y. Wei, S. Rajendran, Y. Zhang, S. Bhattacharya, C. Zheng, Chemical looping combustion of coal in a 5kWth interconnected fluidized bed reactor using hematite as oxygen carrier, Applied Energy, 157 (2015) 304-313.
[67] S. Lin, T. Saito, K. HASHIMOTO, Development of three-tower (reactors) technology for chemical looping coal combustion, in: Proceedings of the 4th International Conference on Chemical Looping, Nanjing, China, 2016, pp. 26-28.
[68] A. Svensson, F. Johnsson, B. Leckner, Bottom bed regimes in a circulating fluidized bed boiler, International Journal of Multiphase Flow, 22 (1996) 1187-1204.
[69] A. Svensson, F. Johnsson, B. Leckner, Fluidization regimes in non-slugging fluidized beds: the influence of pressure drop across the air distributor, Powder Technology, 86 (1996) 299-312.
[70] T. Karlsson, X. Liu, D. Pallarès, F. Johnsson, Solids circulation in circulating fluidized beds with low riser aspect ratio and varying total solids inventory, Powder Technology, 316 (2017) 670-676.
[71] X. Li, A. Lyngfelt, D. Pallarès, C. Linderholm, T. Mattisson, Investigation on the Performance of Volatile Distributors with Different Configurations under Different Fluidization Regimes, Energy & Fuels, (2022).
[72] X. Li, A. Lyngfelt, T. Mattisson, An experimental study of a volatiles distributor for solid fuels chemical-looping combustion process, Fuel Processing Technology, 220 (2021) 106898.

[73] X. Li, A. Lyngfelt, C. Linderholm, B. Leckner, T. Mattisson, Performance of a volatiles distributor equipped with internal baffles under different fluidization regimes, Submitted for publication, (2022).
[74] T. Djerf, Solids Flow in Large-Scale Circulating Fluidized Bed Furnaces, PhD Thesis, Chalmers University of Technology, Gothenburg, Sweden, 2021.
[75] J. Xiang, Q. Li, Z. Tan, Y. Zhang, Characterization of the flow in a gas-solid bubbling fluidized bed by pressure fluctuation, Chemical Engineering Science, 174 (2017) 93-103.
[76] F. Johnsson, R.C. Zijerveld, J.C. Schouten, C.M. van den Bleek, B. Leckner, Characterization of fluidization regimes by time-series analysis of pressure fluctuations, International Journal of Multiphase Flow, 26 (2000) 663-715.
[77] D. Kunii, O. Levenspiel, CHAPTER 4 - The Dense Bed: Distributors, Gas Jets, and Pumping Power, in: D. Kunii, O. Levenspiel (Eds.) Fluidization Engineering (Second Edition), Butterworth-Heinemann, Boston, 1991, pp. 95-113.
[78] S.B.R. Karri, T.M. Knowlton, 4 - Gas Distributor and Plenum Design in Fluidized Beds, 1998.